applied sciences

MDPI

Article

IoT-Driven Resilience Monitoring: Case Study of a Cyber-Physical System

Ali Aghazadeh Ardebili [1,2,*], Cristian Martella [1,*], Antonella Longo [1,*], Chiara Rucco [1], Federico Izzi [1] and Antonio Ficarella [1]

[1] Department of Engineering for Innovation, University of Salento, 73100 Lecce, Italy; chiara.rucco@unisalento.it (C.R.); federico.izzi@studenti.unisalento.it (F.I.); antonio.ficarella@unisalento.it (A.F.)
[2] Department of Research and Development, HSPI SpA, 00185 Rome, Italy
* Correspondence: ali.a.ardebili@unisalento.it (A.A.A.); cristian.martella@unisalento.it (C.M.); antonella.longo@unisalento.it (A.L.)

Abstract: This study focuses on Digital Twin-integrated smart energy systems, which serve as an example of Next-Generation Critical Infrastructures (CI). The resilience of these systems is influenced by a variety of internal features and external interactions, all of which are subject to change following cyber-physical disturbances. This necessitates real-time resilience monitoring for CI during crises; however, a significant gap remains in resilience monitoring. To address this gap, this study leverages the role of Internet of Things (IoT) in monitoring complex systems to enhance resilience through critical indicators relevant to cyber-physical safety and security. The study empirically implements Resilience-Key Performance Indicators (R-KPIs) from the domain, including Functionality Loss, Minimum Performance, and Recovery Time Duration. The main goal is to examine real-time IoT-based resilience monitoring in a real-life context. A cyber-physical system equipped with IoT-driven Digital Twins, data-driven microservices, and a False Data Injection Attack (FDIA) scenario is simulated to assess the real-time resilience of this smart system. The results demonstrate that real-time resilience monitoring provides actionable insights into resilience performance based on the selected R-KPIs. These findings contribute to a systematic and reusable model for enhancing the resilience of IoT-enabled CI, advancing efforts to ensure service continuity and secure essential services for society.

Keywords: IoT-based monitoring; cyber-physical resilience; real-Time; digital twins; empirical study; sustainable energy; smart energy systems; safety-critical systems

Academic Editors: Cristina Stolojescu-Crisan and Fabrizio Marozzo

Received: 5 December 2024
Revised: 27 January 2025
Accepted: 30 January 2025
Published: 17 February 2025

Citation: Aghazadeh Ardebili, A.; Martella, C.; Longo, A.; Rucco, C.; Izzi, F.; Ficarella, A. IoT-Driven Resilience Monitoring: Case Study of a Cyber-Physical System. *Appl. Sci.* **2025**, *15*, 2092. https://doi.org/10.3390/app15042092

1. Introduction

The rise of cyber-physical critical infrastructures (CIs) with advanced features like Artificial Intelligence (AI) integration highlights the importance of assessing and overseeing resilience [1]. These infrastructures require a comprehensive approach to resilience measurement and monitoring due to their complex and interconnected nature. CIs play a crucial role in contemporary societies, covering a wide range of sectors essential for maintaining operations and safeguarding public well-being [2]. These infrastructures are fundamental for the functioning of society and are responsible for delivering essential services to the public. From energy grid CIs to transportation systems, these infrastructures provide essential services that facilitate daily life [3]. Consequently, disruptions in critical systems, such as transportation, communication, and energy, can have far-reaching consequences. For example, disruption in the transportation system could lead to delays

in the delivery of goods and services, resulting in economic losses for businesses and consumers [4]. Similarly, a disruption in the communication system could hinder emergency response efforts and jeopardize public safety [5]. Additionally, disruptions in the energy system could lead to power outages, impacting businesses, hospitals, and individuals who rely on electricity for their daily activities [6,7]. Overall, disruptions in such systems can have cascading effects that threaten public safety and security, as well as causing significant economic losses.

Recognizing the interconnectivity and vulnerability inherent in CIs, it is essential to prioritize resilience in order to mitigate risks and enhance societal resilience when faced with unforeseen challenges. With this approach, communities and societies can better prepare for and respond to various threats and crises, ultimately ensuring their ability to bounce back and recover more effectively [8].

The resilience of CIs is influenced by a wide range of internal characteristics and external interactions, all of which are subject to dynamic changes following cyber-physical disturbances [9,10]. Consequently, resilience must be regarded as a dynamic concept that requires continuous study during crises triggered by extreme events, such as earthquakes or terrorist attacks, and even their aftermath [11,12]. This highlights the critical importance of leveraging IoT technologies for the real-time monitoring of CIs.

In this context, resilience quantification emerges as a crucial approach to understanding, assessing, and enhancing the resilience of CIs. While existing methodologies often rely on metrics and indicators derived from historical data [13–15], a significant gap persists in real-time resilience monitoring. Addressing this gap is essential to effectively capture the dynamic behavior of CIs during crises.

To bridge this gap, this study seeks to answer a pressing and emerging question: ***Is it feasible to monitor the resilience of IoT-integrated CIs in real-time using sensor data for specific KPIs?***

By exploring this question, the study underscores the urgency and relevance of real-time resilience monitoring in advancing the safety and functionality of CIs. Therefore, this article presents an empirical study based on real-world data, observations, and experimentation to derive conclusions. The research design involves developing and operating a cyber-physical testbed to implement various data-driven algorithms for real-time resilience monitoring. The testbed is a smart PV panel, with its resilience being evaluated under a FDIA. The primary contributions of this empirical study are outlined as follows:

- The development and validation of a comprehensive method for real-time resilience monitoring of IoT-integrated CI.
- The implementation and testing of different data-driven algorithms tailored to R-KPIs, informed by observed system behavior.
- The construction and operation of a practical cyber-physical testbed for empirical resilience assessment using a Digital Twin-integrated smart PV system.

The remainder of the article is structured as follows: **Section 2 Research Landscape**: An overview of the current state of resilience assessment of CI. In **Section 3**, we explain the theoretical foundation of the resilience KPIs that are used in this article. **Section 4 Statistical and AI methods**: A detailed description of the cyber-physical system under study and methodology for implementing and measuring the selected R-KPIs. **Section 5 Cyber-Physical System**: A synthesis of the testbed results, with a validation of the resilience monitoring method based on sensor data in the real time. **Section 6 Case Study**: A detailed description of test configuration, and discussion of results from conducted tests results. **Section 7 Limitations, Challenges, and Future Research**: Discussion of study limitations, encountered challenges, and potential future research avenues. **Section 8**

Conclusions: Summarizes key findings and their implications for the resilience monitoring of IoT-enabled CI.

2. Research Landscape

Critical infrastructure (CI) encompasses physical assets and systems that provide a necessary service in national, regional, and local scopes. Because of the necessity of the service continuity of CIs, it is extremely important that the service can be delivered under challenging situations like natural disasters or disturbances from cyber-physical attacks [16].

The capacity to withstand or to recover quickly from risks is called resilience. CI should be resilient in all aspects, from governance to operational level [17].

Prior studies unveiled the efficiency of data-driven solutions to enhance the resilience of complex systems [1,18–20] and CI [21–23]. However, achieving a socio-technical transition towards more sustainable and resilient CIs necessitates substantial conceptual changes in the system architecture, coupled with the incorporation of new assets dedicated to collecting real-time data, communication, and computations. The integration of these new components into the system brings more complexity, consequently diminishing the resilience of the overall system. While this transition seems fundamental because of societal challenges of climate change and increasing natural disasters, emerging cyber-physical threats, and the changes in the service end users' behaviour [24], transforming entire socio-technical CI involves a novel resilience engineering approach [25] to guarantee the uninterrupted service continuity of emerging AI-integrated CIs.

Nevertheless, at present, the technologies supporting these transitions are either under study or in the developmental stage, typically confined to laboratory-scale implementations. Additionally, the majority of existing CIs continue to operate using traditional monitoring and control systems. Therefore, the body of knowledge in AI-integrated CIs resilience engineering is not fully defined, and there is a gap in standardized models and performance metrics to quantify the resilience of AI-integrated CIs.

Next-Gen Energy Systems Resilience

The energy sector is transitioning towards a Next-Gen model, characterized by intelligent energy infrastructures that leverage renewable energy sources [26] and distributed generation [26]. This transformation is further enhanced by emerging technologies such as Digital Twins [19,27,28], IoT, data-driven solutions [28], real-time anomaly detection [29], and big data analytics [30–32], collectively shaping a smart grid that promises a sustainable and efficient future. However, this evolution is not without challenges. Ensuring the resilience of these advanced systems poses a significant challenge, requiring innovative and adaptive solutions. This study is motivated by these challenges and focuses on Next-Gen energy CIs with these defining characteristics.

One key concern lies in the growing dependence on renewables [33,34]. While solar and wind power offer significant environmental benefits, their inherent variability and intermittency pose challenges [35]. Unlike traditional, reliable power plants, renewable sources are not always available, demanding robust energy storage and sophisticated grid management systems to function effectively [36]. Furthermore, extreme weather events can disrupt these already fluctuating sources [37], potentially cascading into power outages and grid instability.

Smart grids, another cornerstone of Next-Gen energy systems, introduce a different set of vulnerabilities. These intelligent networks, enabling two-way communication between utilities and consumers, offer real-time monitoring, dynamic pricing, and improved efficiency. However, the increased complexity creates a larger attack surface for cyber

threats [38,39]. Malicious actors targeting communication networks or control systems could disrupt critical operations, leading to widespread blackouts [40].

The rise of distributed generation, where power is produced closer to consumption points through rooftop solar panels or microgrids, presents a double-edged sword. While it fosters energy independence and reduces reliance on centralized power plants, it also introduces complexities in managing the grid and maintaining stability. Additionally, a cyber-attack targeting a single distributed generation unit could have a ripple effect, impacting the entire grid.

3. Theoretical Foundation of Resilience Curve and Its KPIs in This Domain

To quantify the resilience of smart energy systems, this study conducts a comprehensive literature review. The review identifies various measurable resilience indexes. From this pool of indexes, and various articles, the current study focuses on a case study within smart energy systems. To quantify CI resilience in this CIs, timeliness plays a vital role. Therefore, we prioritize time-related KPIs for this analysis. Other metrics also impact resilience monitoring, such as Age of Information (AoI), which quantifies data freshness and serves as a critical metric for real-time resilience monitoring [41–44]. However, these metrics are not derived from the resilience curve, and we leave their exploration for future studies.

Two reference articles form the foundation for the selection of R-KPIs and resilience curve construction in this study (see Section 3.1 for definitions). An empirical study conducted in the domain of smart PV panels, using a similar testbed [45], serves as a basis for selecting three specific KPIs: functionality loss, minimum performance, and recovery time. To calculate these R-KPIs, it is essential to first construct a resilience curve [46] (see Section 3.1). Given that the collected data are inherently noisy, we apply two methods empirically implemented and evaluated for noisy data in [47]: Support Vector Machine (SVM) and polynomial fitting via least squares (Polyfit) (see Section 3 for definitions). Although SVM was identified in the reference article as the superior method for accurately reflecting system behavior, both methods are employed in this study to allow for comparative analysis. As a practical recommendation for monitoring system resilience, it is advised that once a method is chosen, it should consistently be used throughout the system's lifecycle to construct its resilience curve.

3.1. Resilience Curve and Selected R-KPIs

Resilience curves are widely applied across various fields in resilience engineering, encompassing applications in critical infrastructure resilience [48,49], resilience index development [50–53], recovery reviews [54–57], system component criticality [58–60], post-disturbance activities [61–63], and measurements and/or benchmarking for resilience assessment [64–66].

In this article, the resilience curve will be used to calculate the selected R-KPIs. In the following section, the three R-KPIs that are chosen for further analysis will be defined in detail.

3.1.1. Recovery Time

The primary objective of resilience-enhancing metrics is to enhance the three core capacities of resilience: absorption, adaptation, and restoration. This goal is achieved through the implementation of diverse strategies aimed at strengthening the functionality and performance of critical infrastructure, such as incorporating redundancy.

Redundancy in critical infrastructure refers to integrating duplicate or backup components and systems to ensure that essential functions can persist even in the face of disruptions. By incorporating redundant elements, the system gains the ability to absorb

shocks, adapt to unexpected challenges, and facilitate quicker restoration. Redundancy serves as a safeguard against single points of failure, minimizing the impact of disruptions and significantly contributing to reducing recovery time. It plays a pivotal role in enhancing overall resilience by providing alternative pathways and resources, thereby fortifying the infrastructure's ability to bounce back swiftly and effectively from unforeseen events. Moreover, shorter recovery times can also be achieved through the implementation of measures that prioritize the swift restoration and replacement of impaired infrastructure components. This proactive approach not only accelerates recovery but also contributes to the overall enhancement of resilience, as it minimizes downtime and fortifies the system against prolonged disruptions.

The recovery time after a disruption is a crucial index for critical infrastructure resilience, particularly in sectors like energy, due to its direct impact on overall operational resilience. In the aftermath of a disturbance within critical infrastructure, performance inevitably experiences a decline, reaching its minimum level. Following this critical decrease, there are essentially two potential outcomes. Firstly, the performance may reach zero, resulting in a complete system shutdown—a scenario that is universally deemed unacceptable in any disturbance situation for critical infrastructure.

Conversely, the system's response to the disturbance may trigger a recovery phase, characterized by an upward trajectory in performance levels. This recovery phase is crucial as it signifies the infrastructure's ability to rebound and stabilize after the initial level in performance. The stabilized performance level, as illustrated in Figure 1, can assume one of three forms: it may be equal to the prior stable level, higher than the pre-disturbance level, or lower than the pre-disturbance level. This phase is termed the recovery phase, representing a critical aspect of the system's resilience.

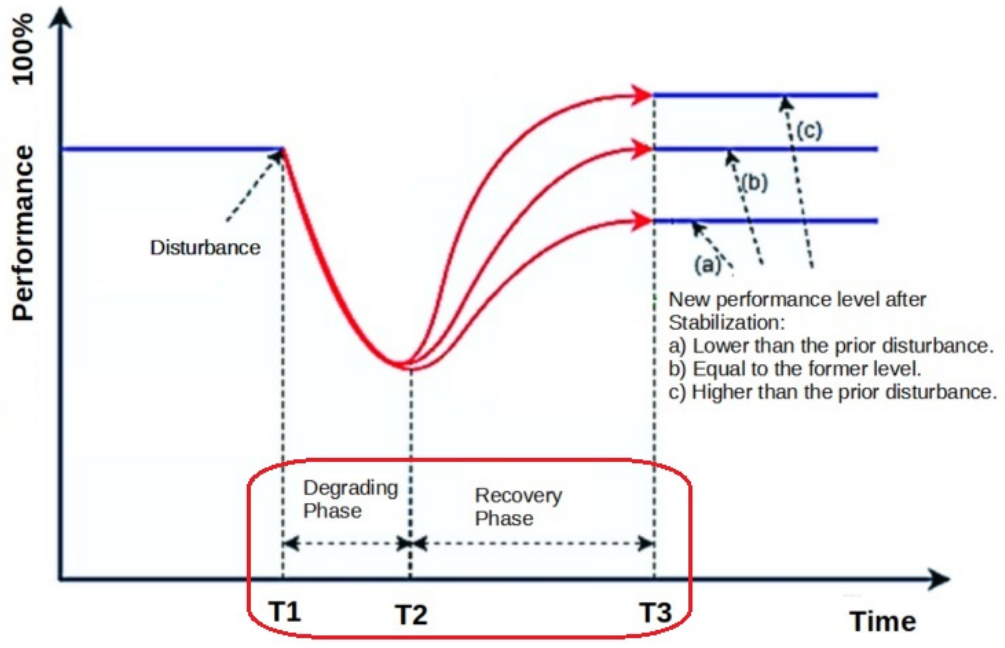

Figure 1. Illustration of recovery time. The red box highlights the point on the resilience curve where the recovery phases duration can be identified.

The concept of recovery time encompasses both the degrading phase, where performance declines, and the subsequent recovery phase, where performance improves and stabilizes. As illustrated in Figure 1, the recovery time spans from the occurrence of the disturbance to the point of stabilization after the recovery phase. The duration of this recovery time is indicative of the system's overall robustness and its ability to efficiently

restore and stabilize its performance following disruptions, which is vital for the sustained and reliable operation of critical infrastructure systems, especially in the energy sector.

3.1.2. Minimum Performance Level

The determination of the minimum performance level in critical infrastructure depends on the inherent design features of the system and the severity of the encountered disturbance. Monitoring this minimum performance level holds crucial significance as it ensures the preservation of essential services vital for the system's proper functioning. The minimum performance level is intricately defined by the indispensable thresholds associated with the societal needs for that particular service. In the event that the minimum performance of a critical infrastructure (CI) descends below this predefined level following a disturbance, it becomes imperative to reassess the response strategy to this risk. Such a proactive approach is essential for safeguarding the reliability and functionality of the critical infrastructure system, aligning its performance with the crucial needs of the society it serves. Continuous monitoring and adaptive strategies are thus indispensable to maintain the resilience and effectiveness of critical infrastructure in the face of dynamic challenges. Figure 2 shows the minimum performance level after disturbance.

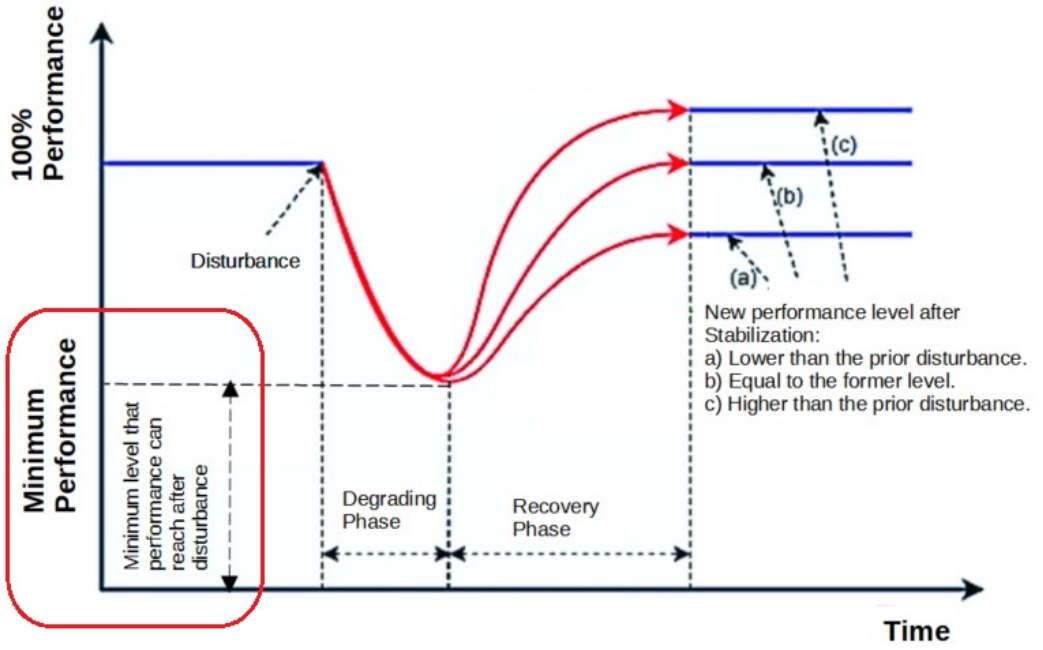

Figure 2. Illustration of minimum performance level. The red box highlights the point on the resilience curve where the minimum performance level can be identified.

3.1.3. Functionality Loss

Resilience curves are applied across the critical infrastructure literature this shows two kinds of curve: a typical representation with a semi-linear degradation and semi-linear recovery phase, or non-idealized system behavior (Figure 3). Since the complex systems can show the irregular behavior after disturbance because the interdependences between other CIs and the dynamic nature and natural complexity of the system, it is important to have a index to cover the loss during the lifecycle of recovery time. This loss is called Loss of Functionality [67]. Figure 4 shows a graphical illustration of Loss of Functionality.

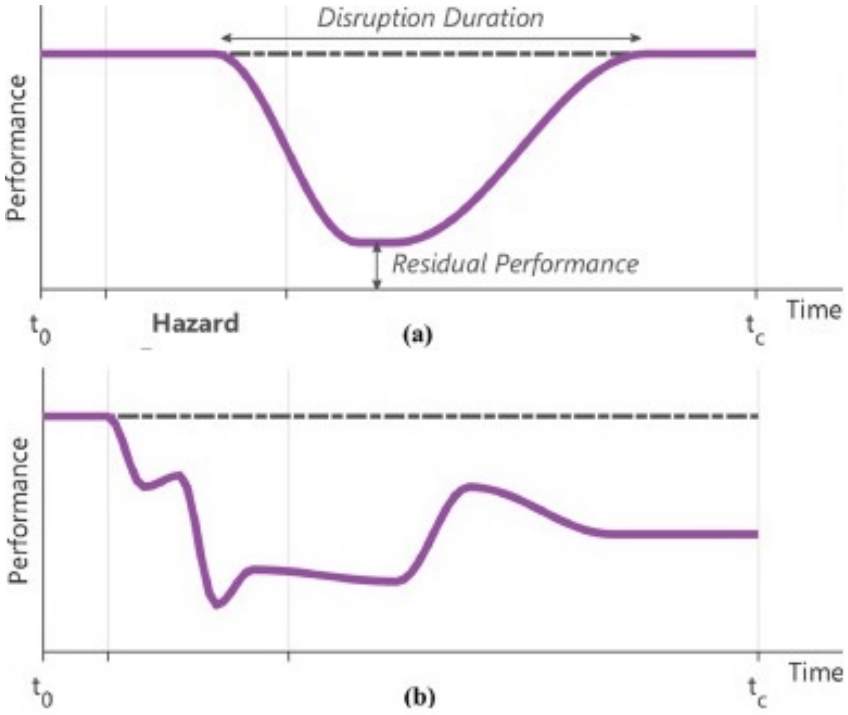

Figure 3. (**a**,**b**) Graphical illustration of different behaviors after disturbance [68].

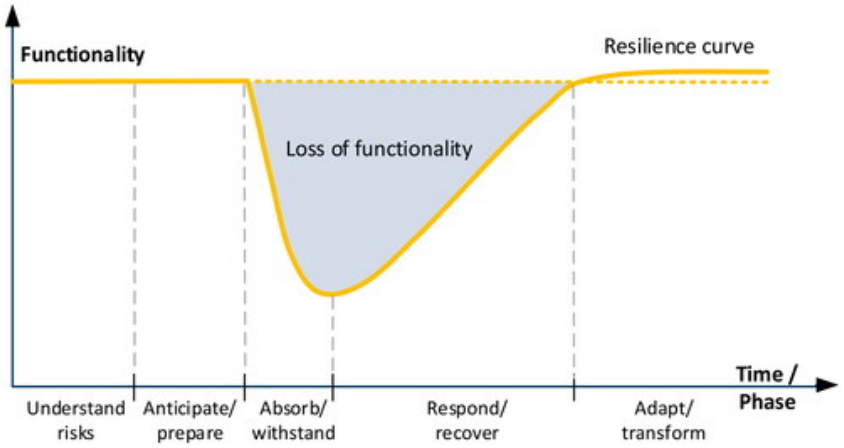

Figure 4. Graphical illustration of Loss of Functionality [67].

The method that is used in this research is adopted from a developed comprehensive framework for assessing the resilience of infrastructure in response to specific events, such as earthquakes [69]. The framework aims to measure the impact of an earthquake by estimating the predicted degradation in the quality of service provided by the infrastructure, denoted as $Q(t)$. We can break down the process:

Assuming a disturbance occurs at time t_0, the degradation in service quality is assessed from the moment of the shock (t_0) until the service quality ($Q(t)$) fully recovers to its pre-disturbance levels at time t_1. This period represents the recovery phase.

The measure of Loss of Functionality, denoted as LF, is determined by considering how much the service quality degrades during the recovery period, regardless of the behavior of the system shown in Figure 3. The calculation can be expressed as follows:

$$FL = \int_{t_0}^{t_1} [100 - Q(t)]\, dt$$

In simpler terms, Loss of Functionality is the difference between the initial service quality at the time of the disturbance (t_0) and the service quality once it has fully recovered (t_1). This provides a quantifiable metric for understanding the impact of the disturbance on the infrastructure's ability to maintain its continuity of service.

4. Implemented Statistical and AI Methods

In the current research, Rolling Average is used for raw data time series smoothing and Polynomial Fitting is employed to model a polynomial that accurately represents the dataset obtained from the testbed during disturbance scenario testing.

Polynomial fitting is a regression technique that fits a polynomial (a mathematical expression consisting of variables raised to powers and multiplied by coefficients) to a set of data points. The goal is to find the polynomial that best captures the relationship between the independent variable(s) and the dependent variable. The degree of the polynomial determines its complexity, and higher-degree polynomials can capture more complex relationships but may also be prone to overfitting.

For Polynominal Curve Fitting, Least Squares Regression and Support Vector Regression (SVR) with a Radial Basis Function (RBF) Kernel model are used. Support Vector Regression (SVR) is a regression algorithm that uses support vector machines to model the relationship between variables. In SVR, the goal is to find a hyperplane that best fits the data while allowing for a certain degree of error. The RBF kernel is a specific type of kernel function used in SVR, and it is particularly effective in capturing non-linear relationships. In the following section, the theoretical foundation of the methods is explained.

4.1. Moving Average

The moving average is a statistical technique used to analyze data trends by smoothing out short-term fluctuations, providing a clearer view of the underlying direction in a dataset [70]. It is particularly useful in time series analysis, where data may exhibit high volatility due to random variations. The most basic form, the Simple Moving Average (SMA), calculates the average of a fixed number of consecutive data points, or "window size". As new data points become available, the average recalculates by including the most recent observation and excluding the oldest one, effectively "moving" along the dataset [71]. For instance, the SMA over a window size N is calculated using the formula:

$$\mathrm{SMA}_t = \frac{X_t + X_{t-1} + \ldots + X_{t-N+1}}{N}$$

where X_t represents the current data point, and N is the window size.

Moving averages have extensive applications across various fields, such as finance, where they are used to identify stock price trends [72], and economics, where they help analyze indicators like GDP and inflation rates [73].

Sensor data from photovoltaic (PV) panels for DC power often exhibits noise due to environmental fluctuations, electromagnetic interference, and sensor limitations. Variations in sunlight, temperature, and shading cause inconsistencies, while electronic components introduce interference, affecting data stability. Sensor inaccuracies, often due to limited sensitivity issues, further contribute to this variability, making it challenging to obtain clean data directly from sensors [74,75].

Implementing a rolling average for smoothing time series data is a widely adopted technique (39,529 documents in SCOPUS used key term `rolling average OR moving average`) with its own set of pros and cons. Rolling averages are a commonly used method for data smoothing and trend analysis [76], offering distinct advantages. Rolling averages have been introduced as a convenient method for regulating power-time curves in

renewable and conventional energy profiles [77–80], which served as the main motivation for considering rolling averages in the current study. Nevertheless, their simplicity may sometimes limit their ability to capture complex patterns in data, highlighting the need to explore alternative or complementary approaches for more intricate analyses.

Recent studies have demonstrated that implementing a rolling average is inefficient for resilience curve construction when data are affected by significant noise [47]. However, in this article, moving averages are used to provide essential smoothing for noisy datasets, making it easier to detect underlying patterns and inform forecasting models [81].

4.2. Least Squares Regression

The polyfit function in NumPy is used for polynomial fitting, which involves finding the coefficients of a polynomial that best fits a set of data points. The theoretical foundation of polynomial fitting lies in the concept of least squares regression.

The goal to minimize the sum of squared differences

$$\text{minimize} \sum_{i=1}^{N} (y_i - P(x_i))^2 \tag{1}$$

In the Matrix form, it can be represented in this way:

$$X = \begin{bmatrix} 1 & x_1 & x_1^2 & \dots & x_1^n \\ 1 & x_2 & x_2^2 & \dots & x_2^n \\ \vdots & \vdots & \vdots & \ddots & \vdots \\ 1 & x_N & x_N^2 & \dots & x_N^n \end{bmatrix} \quad C = \begin{bmatrix} c_0 \\ c_1 \\ \vdots \\ c_n \end{bmatrix} \quad Y = \begin{bmatrix} y_1 \\ y_2 \\ \vdots \\ y_N \end{bmatrix}$$

Finally, a solution is gained using least squares

$$C = (X^T X)^{-1} X^T Y \tag{2}$$

4.3. Support Vector Regression (SVR) Model with a Radial Basis Function (RBF) Kernel

$$f(x) = \sum_{i=1}^{n} \alpha_i K(x, x_i) + b \tag{3}$$

where $f(x)$ is the predicted output, n is the number of support vectors, α_i is the coefficients associated with the support vectors, $K(x, x_i)$ is the kernel function, which measures the similarity between x and the support vectors x_i, and b is a bias term. The RBF kernel is defined as follows:

$$K(x, x_i) = \exp\left(-\frac{\|x - x_i\|^2}{2\sigma^2}\right) \tag{4}$$

where σ is a parameter that controls the width of the Gaussian distribution.

This equation captures the non-linear relationship between input features and output in the SVR model. The specific form of the kernel function, in this case, the RBF kernel, contributes to the model's ability to capture complex patterns in the data.

It should be noted that the SVR model is designed to handle non-linear relationships and may not have a simple linear equation like traditional linear regression.

5. Cyber-Physical System

This section includes the discussion of a real case study that we have implemented to assess the energy CP framework that we propose. Being a prototype, the case study should be considered as an experiment in which the building blocks were implemented according to the essential functionalities and features they must provide. As already

mentioned, our ambition is to perform a complete testbed of the proposed framework in order to assess the same framework. The architecture adopted for the case study is shown in Figure 5. According to the proposed energy CP framework, it includes the three main building blocks: Physical Asset, Data Infrastructure, and Digital Twin. The Physical Asset consists of a portable power-generating infrastructure in an autonomous Smart PhotoVoltaic Station that features a PV panel equipped with sensors to assess the placement surrounding's conditions, along with actuators to control the orientation of the panel. The Data Infrastructure is limited to implement two fundamental services for the framework, which are data streaming and data persistence. For the case study, the device we have adopted for deploying these services is a fog node implemented by a Raspberry PI 4B. Finally, the Digital Twin was implemented in the form of a virtual world interactive model of the SPVS. According to the proposed framework, the overall Digital Twin includes its four fundamental services, which are Dynamic Environment, Operation, Ideal State, and Demand. Considering the processing and storage resources the Energy DT needs, these services are deployed on a workstation. Such a workstation represents the cloud backend of the framework we propose, but with more limited resources in terms of processing and storage capabilities.

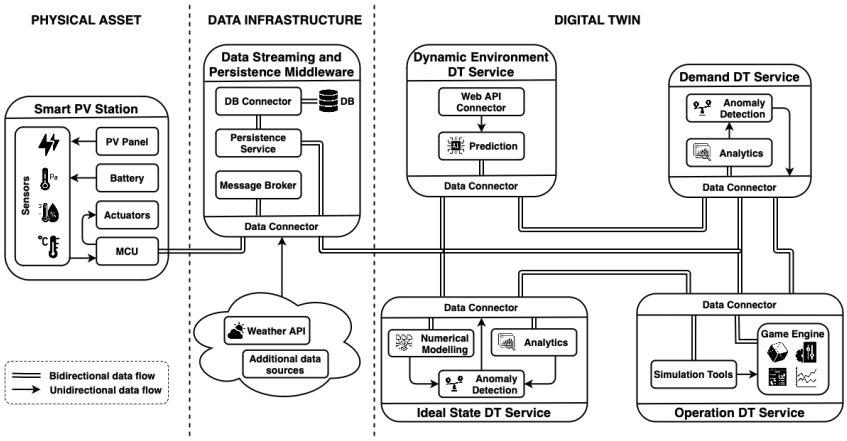

Figure 5. Conceptual model of the proposed system [82].

5.1. Physical Asset: Smart PhotoVoltaic Station

The models discussed in this case study are applied in the PV power generation system called a Smart PhotoVoltaic Station (SPVS). Such a system is part of the real testbed we have conducted and which is detailed in the present section. The list of components that are presented in Table 1 was used for assembling the CP infrastructure (Figure 6a,c) and for evaluating our experimental setup.

Table 1. List of sensors, actuators, and other components [45,82].

Category	Component	Specification
Sensors	Air quality	Bosch BME280 (Bosch Sensortec GmbH, Reutlingen, Germany)
	Power	INA3221
Actuators	Servo motors	2× (0°–180°)
Other Components	MCU	2× ESP32
	Voltage converter	2×
	MPPT	
	Battery	LiFePo4 12 V 6 Ah
	PV panel	20 W monocrystalline

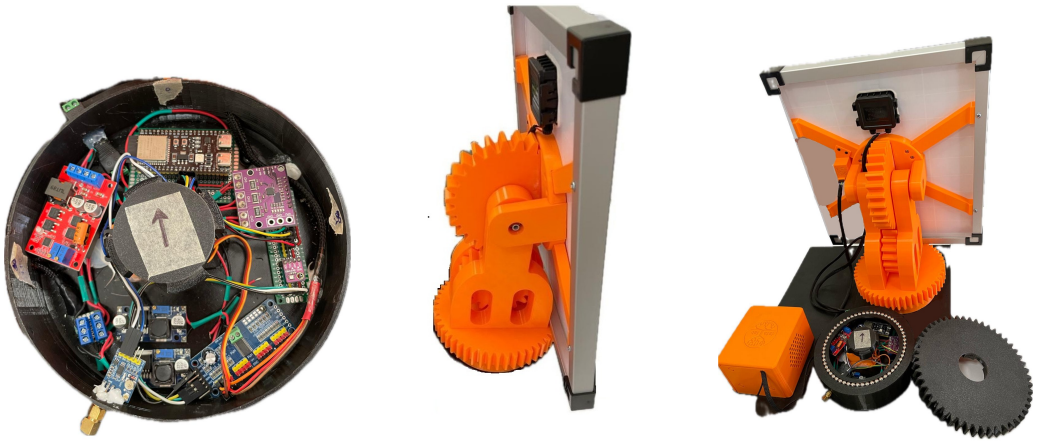

(**a**) (**b**) (**c**)

Figure 6. SPVS physical asset implementation. (**a**) Control system (Table 1). (**b**) Motion mechanism. (**c**) Assembled view (back view).

The logical model of the SPVS is shown in Figure 7, where the physical components and the connections between them are represented. In particular, it includes two types of physical connections: power delivery and data delivery. The former is used to highlight the electric circuit to power the SPVS components, whilst the latter maps the data streams between the components.

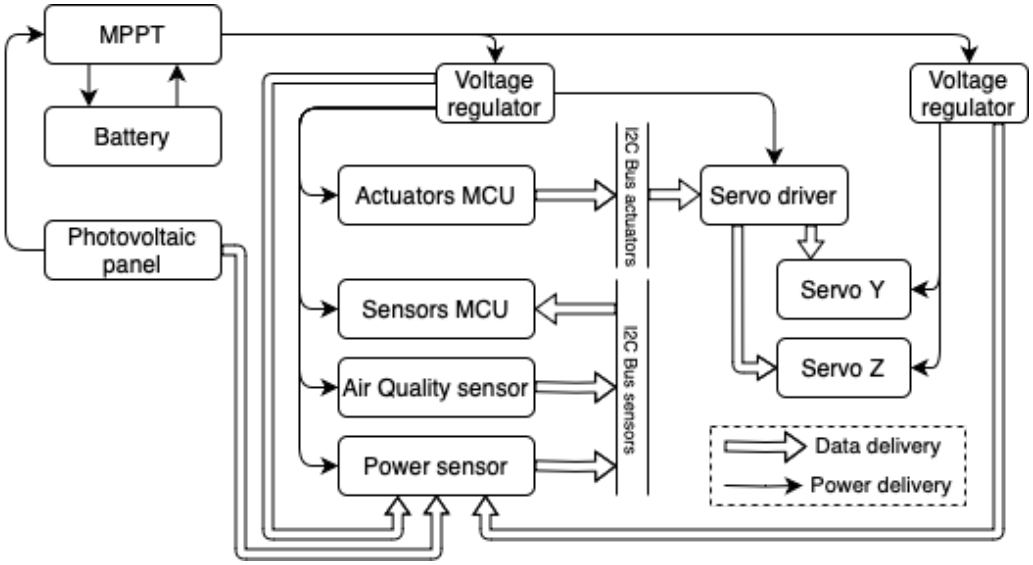

Figure 7. The logical model of the smart PV system [45,82].

5.1.1. PV Panel

For the purposes of this work, the choice of a suitable PV panel plays a critical role. Since the module is used for a portable SPVS as a testbed, a 20 W monocrystalline solar module has been chosen. Moreover, durable ESG glass is another relevant requirement to avoid the degradation of the module due to microfractures during installation and movements of the PV panel.

The 20 W Mono Solar Module from Offgridtec (MPN 3-01-001560), whose datasheet is shown in Table 2, operates with high-efficiency monocrystalline solar cells (>18%), and thanks to its operating voltage of 20 V, it is ideal for 12 V systems. "Monocrystalline" refers to a type of solar cell or module where the silicon used in the construction is made

up of a single crystal structure. In contrast, polycrystalline solar cells are made from multiple crystals, and thin-film solar cells are made using different materials altogether. Monocrystalline solar cells are known for their higher efficiency and greater space-efficiency compared to other types.

Table 2. Offgridtec Mono20W3-01-001560 PV module specifications.

Parameter	Value
Maximum Power (Pmax)	20 W
Open Circuit Voltage (Voc)	22.3 V
Short Circuit Current (Isc)	1.21 A
Voltage at Maximum Power (Vmpp)	17.8 V
Current at Maximum Power (Impp)	1.12 A
Module Efficiency of Voc	−0.45%
Module Efficiency of Isc	−0.45%
Module Efficiency of power	−0.45%
Nominal Operating Cell Temperature (NOCT)	45 (± 2) °C
Operating Temperature Range	−40 °C to +85 °C
Cells type/Array	2 × 18
Maximum system voltage	600 VDC

Values are measured at Standard Test Conditions (STC), with Irradiance 1000 Wm^{-2}, Air Mass (AM) 1.5 Spectrum and Temperature 25 °C.

5.1.2. Sensors and Actuators

The SPVS features a set of sensors and actuators used to perceive and interact with the surrounding environment. On the sensors side, the device is equipped with sensors to assess the air quality (temperature, atmospheric pressure, and relative humidity) and a DC power sensor that is used to collect data on the live power production of the PV panel, the power stored in the battery, and the power used by the system in performing its operations.

The station is also capable of tracking a desired orientation. To do so, on the actuators side, the device's mechanical gear work is actuated through a couple of servo motors. One of them is devoted to control the pitch angle of the panel, whilst the other one controls its yaw angle (as shown in Figure 8).

5.1.3. Service Modules

The brain of the SPVS physical asset is implemented through ESP32 micro-controller units (MCU). The choice of this chip is motivated by its good performance, relative to the requirements posed by tasks it is intended to perform and the services it should expose, at a low price and bundled in a tiny board. The ESP32 board also includes an antenna module that allows it to establish wireless communication (either WiFi or Bluetooth) on the 2.4 GHz band.

The device is powered using the energy generated by the PV panel and stored in the accumulation system. In particular, a Maximum Power Point Tracker (MPPT) is used to monitor the output of the PV panel and adjust the voltage and current so as to keep the system always at the point of maximum power. The output of the MPPT feeds the battery, but it is too high to power the logical components that require at most 5 volts. Additionally, it is also important to split the power sources to use for low power (sensors and control devices) and high power (servo motors) devices, respectively. Therefore, two step-down voltage converters are installed between the system's power source output (the battery) and the modules that need to be powered. These step-down voltage converters are tuned to output constant 5 volts. By keeping the power sources separated, it is possible to avoid undesired power drops when performing power intensive tasks that would result in the reboot of the MCU board or even the damage of the most sensitive components.

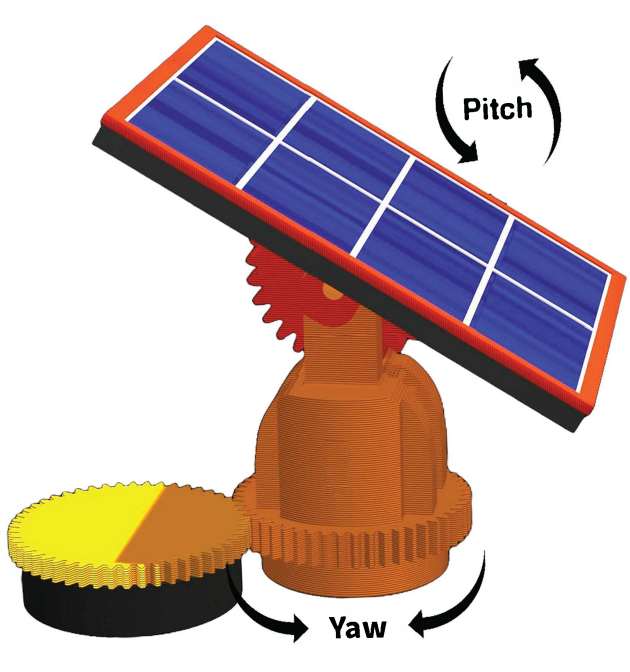

Figure 8. Dynamic 3D model with 2 degrees of freedom (Dof) that is used to visualize the current gradient of the PV module [45,82].

5.2. Data Infrastructure: Data Streaming and Persistence Middleware

For the purpose of the present case study, the Data Infrastructure component of the proposed framework is delegated to the exclusive management of data streaming and data persistence. The Data Streaming and Persistence Middleware (DSPM) is crucial because it allows the exchange of data within the CP system by determining how these data must persist and how they must be made available to both the Energy DT's services and the SPVS. Moreover, the DSPM is responsible for retrieving additional data by issuing specific requests to external data sources. For the present case study, the contributions obtained by these external data sources are related to services like open weather APIs (for obtaining instantaneous weather metrics), but also additional IoT sensors, such as local weather stations and pyranometers. The software module that implements the interface with external data sources is called Web API Connector.

A detailed discussion about the services corresponding to data streaming and data persistence is reported below.

5.2.1. Data Streaming

The data streaming service makes it possible the interaction between the SPVS and the virtual world interactive model. Such an interaction was implemented by adopting the Message Queuing Telemetry Transport (MQTT) protocol that enables the publish/subscribe paradigm. The efficiency of MQTT at an industrial scale has been demonstrated in previous studies [83]. In this regard, an instance of message broker was made available to support the communication between MQTT publishers and subscribers. Clients subscribe to MQTT topics to secure sensor data payloads, ensuring timely data reception, concurrent with the publishing activities. Incoming messages undergo a deserialization process, transforming payloads into manipulable JSON objects for data extraction and subsequent processing.

On the service side, the software module of the case study architecture that is delegated to support data streaming between services is called *Data Connector*. The Data Connector operations flowchart is reported in Figure 9. So, all the services of the framework that must be enabled for the data streaming needs to integrate such a module. In addition,

the data streaming service is responsible for managing communication via the message broker and the reference database instance, as well as acquiring data from the SPVS and the Energy DT's services. This result is achieved by using an approach to a data fetching request that can be configured to be synchronous or asynchronous, as needed. In this way, it is possible to integrate a controller to the software components of the edge device which can regulate the data transmission rate by monitoring specific indicators related to the state of the system, such as the battery level of charge. A specific service of the middleware called *persistence service* intercepts the MQTT traffic between the SPVS and the virtual world interactive model in order to persist the corresponding data entities.

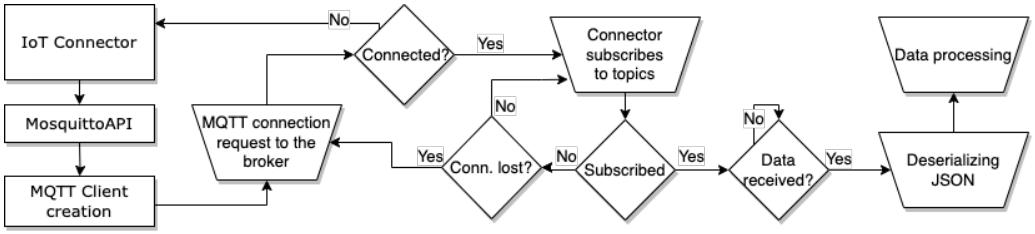

Figure 9. Data Connector flowchart.

5.2.2. Data Persistence

The Data Persistence service consists of two microservices that make it possible to store historical records of data flowing back and forth between the the SPVS and the Energy DT's services, namely sensor readings and action commands. These two microservices implement the interface and the interaction with the reference DBMS instance. Among the possible database solutions, MongoDB was identified as the most suitable for the case study, thanks to its document-based nature that fosters high performance querying of IoT data [84] alongside an efficient handling of several insert queries. When comparing to relational DBMSs such as MySQL, MongoDB allows to outperform in terms of resources usage and overall latency [85,86].

MongoDB's document-based approach allows to store and process heterogeneous data types, such as sensor data, time-series data, and metadata, in a single document. Supporting an efficient and effective local data storage on edge devices, MongoDB allows to reduce the need to stream data towards remote servers or cloud infrastructures. Concerning the DBMS interface microservice, a Python script represents the most suitable solution for the present case study in terms of disk usage and responsiveness performance. Indeed, the usage of state-of-the-art software solutions, such as Apache NiFi, can be counterproductive and challenging due to the high computational needs they require to run on the resource-constrained fog device used for the testbed. A Python script provides a subscription for each MQTT topic related to both the physical and the digital counterpart, acting as a man in the middle. In this sense, it intercepts the corresponding data flows exchanged by the two counterparts and prepares the carried data entities for storage by interacting with the MongoDB microservice.

5.3. Energy Digital Twin: Virtual World Interactive Model

According to the CP framework proposed in this work, the DT corresponds to the digital counterpart of the physical asset. For the aim of the case study, we have implemented the DT as the Virtual World Interactive Model of the SPVS. Such a model corresponds to an interactive and graphical representation of the SPVS within the Unreal Engine virtual world. By following the specification of the framework we propose, the Energy DT provides four interconnected services called *Dynamic Environmental Service* (DES), *Operation Service* (OS), *Ideal State Service* (ISS), and *Demand Service* (DS), respectively. A detailed description for each of these services is provided in the following section.

5.3.1. Dynamic Environment Service

For the present case study, the DES service is delegated to gather environmental data detected by the sensors installed on the SPVS, along with meteorological data retrieved by the DSPM, using a Web API Connector. Regarding this former aspect, DES collects basic environmental parameters like temperature, pressure, and humidity, but also additional weather information, including cloud coverage and solar irradiance relative to the location where the SPVS is installed. The DES service processes the collected data to perform predictions on temperature and irradiation using ML approaches. Finally, it assimilates solar radiation metrics, which encompass values related to Direct Radiation, Diffuse Radiation, and Direct Normal Irradiance.

5.3.2. Operation Service

The OS service is driven by the system's functioning based on embedded sensors and real-time data to simulate production and the current state of the physical asset. Such a service carries out a series of tasks such as the following: (1) ensuring the real-time simulation of dynamic environmental conditions by referring to environmental data detected from its deployment location, (2) employing AI methods to forecast the values of environmental parameters, and (3) feeding these predicted values to the ISS to estimate both the ideal state of the system and the corresponding actual production, using real-time data analytics. The OS service represents a central node for the CP system that interfaces with the SPVS's physical components and synthesizes data from various Energy DT services, external APIs, and embedded sensors. The OS service utilizes software modules for implementing system interaction and data visualization. By observing Figure 5, it is possible to note that the OS includes a software module called *Game Engine* (GE). The GE consists of an instance of Unreal Engine and is responsible for rendering the high-fidelity virtual model. It offers a real-time graphical representation of the physical asset's digital counterpart. This graphical representation is more than a mere visual representation, considering that it enables functional simulations, providing an interactive platform that mirrors the SPVS's physical state and behavior. The GE component plays a pivotal role for the proposed framework because it provides a graphical representation of the DT and the corresponding digital representation of the current state of the physical asset at the same time. It merges field data obtained from the SPVS and data received from other Energy DT's services to process and exhibit the corresponding results, using intuitive dashboards and illustrative charts. These dashboards and charts provide a detailed snapshot of real-time data, enriched by the valuable predictions generated by the Energy DT's services dedicated to the delegated predictive analytics to achieve this goal.

The OS service operates a convergence between data directly obtained from embedded sensors of the SPVS and data streams coming from other Energy DT's services. It orchestrates this information into detailed analytical visualizations and an accurate representation of the physical state. Among the assimilated data, the OS receives detailed anomaly effects such as shading and soiling on the PV panel. This specific information, coupled with weather-related data retrieved from the DSPM component, prompts the OS service to render an approximate cloud condition and its consequent impact on light physics. Moreover, it utilizes forecast data from the other services of the Energy DT to perform simulations predicting future conditions. This predictive information is effectively used to generate visual comparisons through specialized graphics and dashboards (see Figure 10). These visualizations enable a direct comparison of real-time operational data with predicted outcomes, providing a layered and comprehensive perspective on the system's functionality.

Figure 10. Interactive Platform Interface [82].

The OS service establishes a real-time bi-directional communication with the SPVS to facilitate the monitoring of the current state of the physical asset and the manual tuning of a set of parameters. In this way, both the state of the digital and physical assets are synchronized and it is possible to interact with the physical SPVS by executing direct commands through the dashboard made available by the user interface rendered in the Unreal virtual world.

Finally, the OS service facilitates bidirectional communication with the SPVS, enabling its direct control. In this way, it becomes possible to (1) accentuate the synergy within the CP infrastructure, (2) empower the dynamic interaction with the SPVS, and (3) ensure optimized performance through continuous monitoring and immediate control adjustments, based on the system's data-driven insights.

5.3.3. Ideal State Service

The ISS provides anomaly detection functionality within the SPVS. Anomalies are characterized by a number of factors such as soiling, shading, CP attacks, and component malfunctions, which require fast and accurate detection in order to optimize the performance of the system and guarantee the service continuity.

The ISS is meant to estimate the ideal production parameters for a given set of real-time factors, including temperature, solar irradiation, and energy demand. Such an estimate can be carried out either analytically, i.e., using a mathematical model of the SPVS equivalent circuit [87], illustrated in Figure 11, or using a ML model trained on real-world data.

The ISS compares the estimated values of current (I), voltage (V), and power (P) with the measured set of corresponding parameters provided by the OS. If a gap between the two sets of parameters crosses certain defined tolerance thresholds, an anomaly is detected. The event diagram illustrated in Figure 12 illustrates the process of estimation and comparison implemented by the present service.

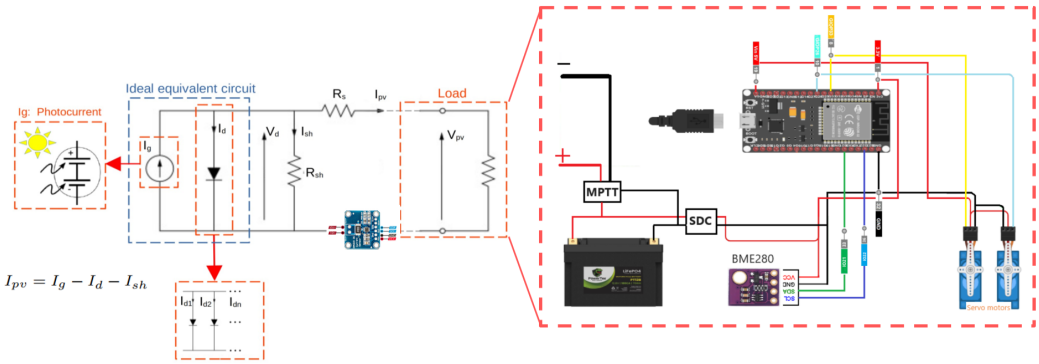

Figure 11. The equivalent circuit of the PV module with the load.

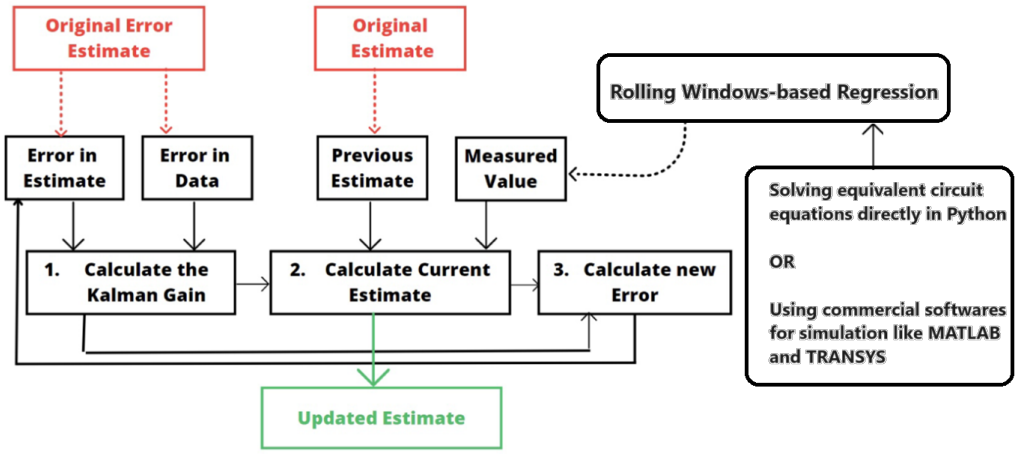

Figure 12. The block diagram of Kalman filter method that is used in current approach.

In particular, the estimation of production values involves numerical models based on the solution of the set of differential equations reported below (note: In Equation (5), I_{pv} is the output current of the PV cell, I_g is the actual photocurrent, I_d is the current of the diode, and I_{sh} is the current of the shunt resistor, K_i is a parameter provided in the datasheet or technical documentation of a specific photovoltaic device or solar cell, I_{gn} is photocurrent STC (Standard Test Condition), G is the actual irradiance, $G_n = 1000$ [W/m^2], the irradiance at STC, K_i is the temperature coefficient, and T is the actual temperature in Kelvin. T_0 is the temperature STC (typically 298 Kelvin), V_T is the thermal voltage, calculated as $(K * T)/q$, K is the Boltzmann constant = $1.3806503 \times 10^{-23}$, J/K, T is the actual temperature of the p-n junction in Kelvin, and q is the elementary charge = $1.60217646 \times 10^{-19}$, C).

$$\begin{aligned} I_{pv} &= I_g - I_d - I_{sh} \\ I_{\mathrm{d}} &= I_0\left(e^{\frac{V}{nV_T}} - 1\right) \\ I_{\mathrm{g}} &= I_{\mathrm{gn}}\left(\frac{G}{G_n}\right)(1 + K_i(T - T_0)) \\ I_{\mathrm{sh}} &= \frac{V_{\mathrm{oc}}}{R_{\mathrm{sh}}}\left(1 - \exp\left(\frac{qV}{nKT}\right)\right) \end{aligned} \tag{5}$$

By solving these equations, it is possible to assess the data for the system functioning in totally ideal conditions. However, real-world data are inherently dynamic and non-linear. Data collected from real-world systems inevitably contains noise, introducing uncertainty around the signal value. To enhance the robustness of the estimation process, a real-world-similar synthetic data generation approach is employed, based on the methodology introduced and described in [88,89]. This approach helps with ensuring

that there is a more reliable estimation of production values, simulating the impact of noise in data acquisition systems into data. In particular, the process involves a Rolling Window Regression algorithm that is initially trained with noise-free synthetic data. Noise is then introduced to the estimated data using various distributions and, subsequently, a Kalman filter is applied to filter the noisy data, as illustrated in the flowchart in Figure 12. Finally, the optimal distribution is selected based on the best Mean Squared Error of the AI algorithm, recognizing that different distributions may better suit each parameter. As a result, a dataset that contains I, V, and P values for different temperatures and irradiation is built. Then, by using a Python script, the nearest temperature and irradiation in the dataset are identified and the corresponding ideal I, V, and P for the given conditions are extracted. Eventually, these values are compared with the actual values from OS to discern disturbances in the system and trigger anomaly detection warnings in the interactive platform's interface (Figure 10).

5.3.4. Demand Service

The DS is responsible for forecasting the energy consumption of appliances and attached AC devices and inferring the configuration of the SPVS to optimize a given cost function, improving the energy management task. This data-driven approach requires means to collect valuable field data to be used, in turn, as the input for properly tuned ML models. To enable this functionality, on the physical asset side, the basic setup of the SPVS described in Section 5.1 should be expanded with an inverter module connected to the output of the MPPT module. The inverter enables DC to AC current conversion, allowing to feed AC loads. An AC power sensor can be installed on the load to monitor and collect data regarding the energy demand footprint.

Data from DES and OS (discussed in Sections 5.3.1 and 5.3.2, respectively) are merged with field data from AC power sensors to feed ML models capable of forecasting the evolution of the power demand and enabling the analysis of what-if scenarios to support the decision-making process and optimize the power generation in different conditions.

5.3.5. Service Deployment

The framework services of the SPVS architecture (see Figure 13a) were organized and distributed by following the principles of the edge cloud continuum [82] and according to the European Scope of the Cloud-Edge computing [90]. In particular, the CP infrastructure was developed in the works of [82,91] as a testbed and features the physical asset, an on-premise edge node, and a desktop data center (as illustrated in the simplified logical schema in Figure 13b).

By following the original approach, data monitored by the SPVS are upstreamed to the on-premise edge node, which acts as a proxy between upstream data consumers and downstream physical entities. The role of such node is to perform the preliminary data preparation pipelines, enhancing the data quality and making data available in the right format. Upstream, the desktop data center models a far edge (near-premise) data center, as presented in [90]. Offering more computational resources, this data center can perform heavy and complex analyses and predictions on relatively limited batches of data streamed by on-premise edge nodes. Following this approach, it becomes possible to implement a local-level policy decision tool, whose purpose is to perform informed decisions based on analyses, other than implementing fine-grained strategic actions. The results obtained by these strategic actions can be then translated to commands for the managed downstream physical devices.

When required, heavier analyses can be delegated to the cloud infrastructures and eventually using the corresponding results to provide global insights and assess optimization policies on an aggregated level-scale.

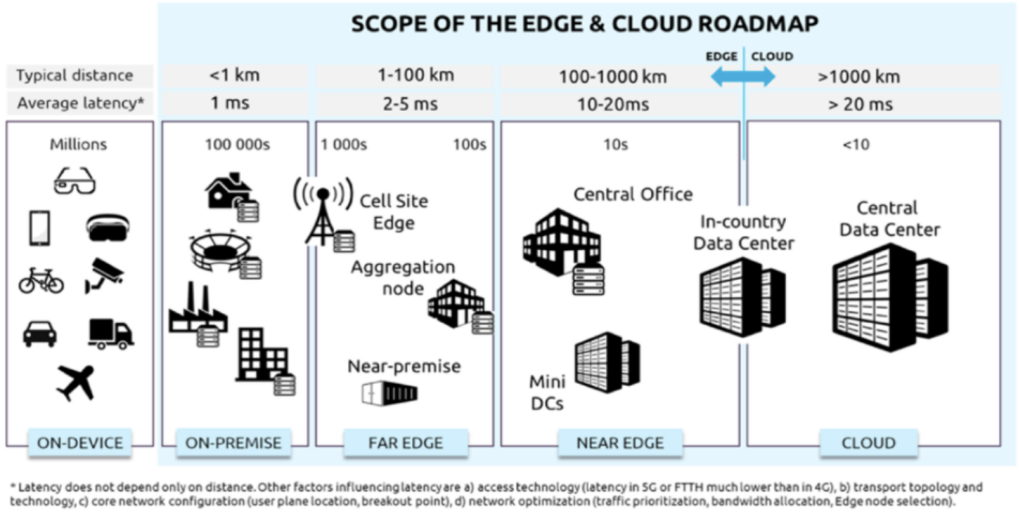

(**a**)

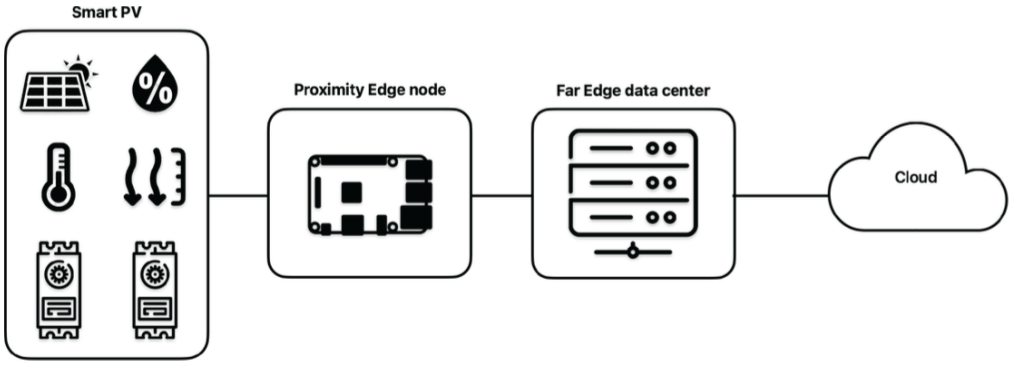

(**b**)

Figure 13. Mapping of the Edge-cloud architectural framework. (**a**) Scope of the European Industrial cloud and edge Roadmap [90]. (**b**) Edge-cloud architecture of the system [82].

Furthermore, the high flexibility and scalability of such a distributed design fosters the development and deployment of resilient cyber-physical systems, encouraging the implementation of efficient resilience boost techniques tailored to the requirements of the specific edge-to-cloud layer that they are applied to.

The R-KPIs encompass three key metrics, as reported in Table 3.

Table 3. Selected R-KPIs.

R-KPI	Definition	Significance
Recovery Time (T)	Represents the duration required for the system to recover from a disturbance occurrence.	Provides a quantitative measure, shedding light on the system's ability to rebound following an event.
Functionality Loss (FL)	Illustrates the extent of functionality loss in the system, irrespective of the system's behavior during degradation and recovery.	Offers insights into the overall impact on system functionality, encompassing both observable and latent effects.

Table 3. *Cont.*

R-KPI	Definition	Significance
Minimum Performance (Pmin)	Indicates the minimum level of performance achievable by systems.	The rationale for utilizing this index lies in the complexity of fitting the resilience curve to the dataset derived from IoT sensors embedded in the system. The intricate behavior of the system post-disturbance may lead to the loss of local and global minimums in performance degradation during the polynomial fitting of the curve (refer to Figure 2). The Minimum Performance Index is instrumental for decision-makers, enabling them to consider the critical threshold of minimum acceptable performance in crucial infrastructures.

The justification for employing the Minimum Performance Index underscores the challenges associated with fitting resilience curves to IoT sensor data and the intricate behavior of the system post-disturbance. This index serves as a vital reference point for decision-makers, allowing them to factor in the minimum performance crucial for the resilience of CI.

6. Case Study

In the present section, we analyze the outcomes of the implementation of the selected R-KPIs to evaluate the overall functionality of the system by examining data gathered from the embedded sensors of a smart PV panel. Various tests were conducted during brief periods throughout the day, encompassing diverse time frames and varying weather conditions. The current section synthesizes the data collected on December 18th. The remainder of this section is structured as follows: Section 6.1 presents the daylight and other pertinent environmental conditions on the test day; the test procedure is documented in Section 6.2 and the disturbance scenario is detailed in Section 6.3; Section 6.4 discusses the testbed functionality validation; finally, the resilience quantification is analyzed in Section 6.5.

6.1. Test Condition

The date of 18 December 2023 was selected for the tests because the weather remained generally clear with occasional cloud cover. We go into more detail in the following section:

Overall, the weather conditions were suitable, with no significant variations in temperature or visibility. The day featured mostly clear skies, transitioning to partly cloudy in the afternoon, and the wind speeds remained moderate throughout the observed period. These conditions were favorable for conducting tests and collecting data as part of the system implementation (the detailed environmental data are collected from https://weatherspark.com/).

- **Temperature:** Ranged from 11 °C to 14 °C.
- **Atmospheric Pressure:** Maintained at around 1030 to 1034 hPa.
- **Wind:** Predominantly from the NW direction, with speeds varying from 17 to 31 km/h.
- **Visibility:** $\geq$10 km throughout the day.
- **Cloud Cover:** Mostly clear and partly cloudy, with occasional cloud layers at 450 to 600 m.

- **Dew Point:** Varied between 9 °C and 11 °C.

Figure 14 shows the elevation of the center of the Sun above (positive) or below (negative) the horizon (black line). Yellow and gray fills indicate day and night, respectively. Light gray lines are the corresponding curves for the winter and summer solstices. Civil twilight and night are indicated by shaded overlays. Figure 15 provides more details related to Monday, 18 December 2023 in Lecce (Italy) (the portable smart PV power station testbed is situated within the Ecotekne complex, located in Lecce, Italy. The geographical coordinates are 40°19′59.2″ N latitude and 18°06′51.3″ E longitude). These details can be defined as follows: cloud coverage (color coded by percentage of sky covered), height of dominant cloud layer (black dots: report time; lines: inferred duration), and any other cloud layers (gray dots and lines). Finally, Figure 16 details the following: measured temperature at approximately 2 meters above the surface of an open field (black dots); 6-, 12-, and 24-hour lows (horizontal blue lines) and highs (red lines), placed above the hourly average temperature (faint purple line), with 25th to 75th and 10th to 90th percentile bands. The thin dotted line is the perceived temperature. Civil twilight and night are indicated by shaded overlays.

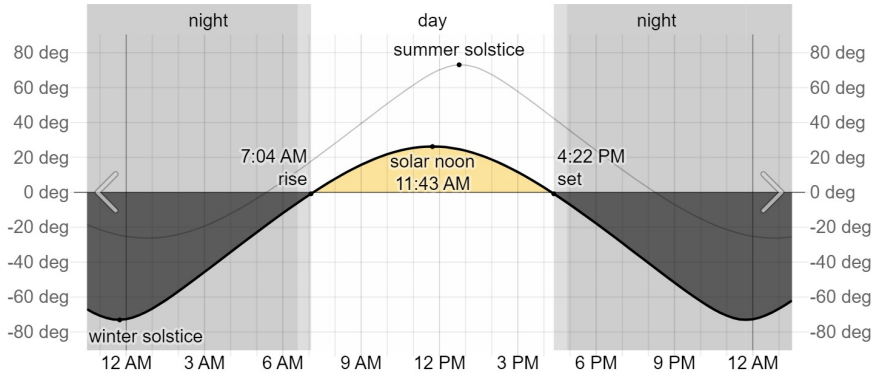

Figure 14. Solar Elevation on Monday, 18 December 2023 in Lecce.

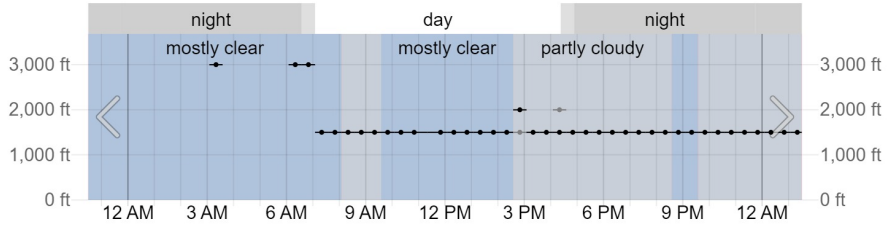

Figure 15. Cloud Cover on Monday, 18 December 2023 in Lecce.

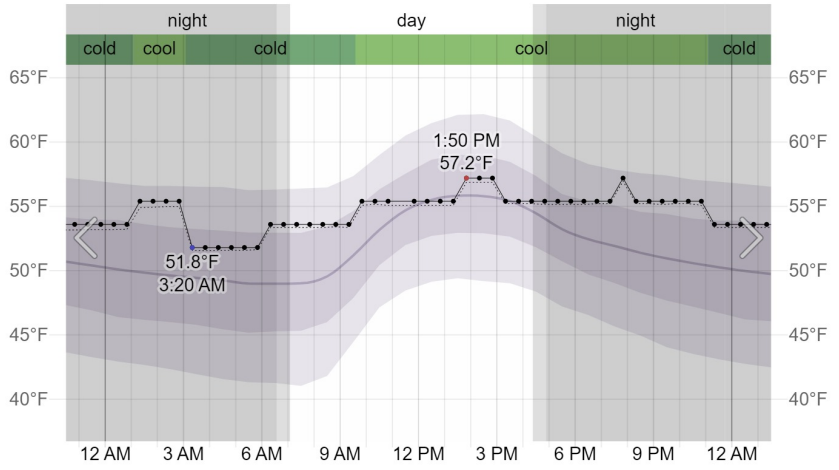

Figure 16. Temperature on Monday, 18 December 2023 in Lecce.

6.2. Test Procedure

The smart PV panel is positioned at the position that is in Section 6.1 for evaluating its general functionality. The testing procedure involves comprehensive data collection throughout the day, which is subsequently compared against solar energy availability and prevailing weather conditions. This comparative analysis aims to ascertain whether energy production aligns with daylight patterns and adapts to the dynamic environmental factors such as the cloudiness.

Given the system's design to trace the sun's trajectory, the hypothesis posits that the smart PV panel is supposed to achieve peak capacity throughout the day until sunset, coinciding with a general reduction in irradiation. Correspondingly, a decline in energy production is expected along with diminishing irradiation. Conversely, during periods of cloudiness or partial cloud cover, an observable oscillation in energy production is anticipated.

The verification of these hypotheses in the experiment involves a visual examination of the dynamic environmental conditions alongside energy production. Future studies to assess production accuracy could involve constructing data-driven or physical models of the system, utilizing tools such as MATLAB Simscape or PVlib Python toolbox. The comparison of actual production against the model-based simulation of production will provide a method for evaluating system performance.

Furthermore, these future studies will offer the potential to gain insights into the noise present in data originating from embedded sensors. Therefore, such further exploration can unveil the real-world behavior of the system under dynamic environmental conditions, shedding light on the impact of various sources of noise. In the next subsection, the results of the tests and the collected data are reported and discussed.

The test began at 7:46 in the morning and ended at 17:08, involving continuous data collection. Figure 17 illustrates the bus voltage values of the panel in volts. The data were recorded at a frequency of every 30 seconds. In Figure 18, the original dataset is depicted alongside a line plot that incorporates a rolling average (with a window size of 10). This rolling average ensures a smoother curve, facilitating a more nuanced analysis of the data.

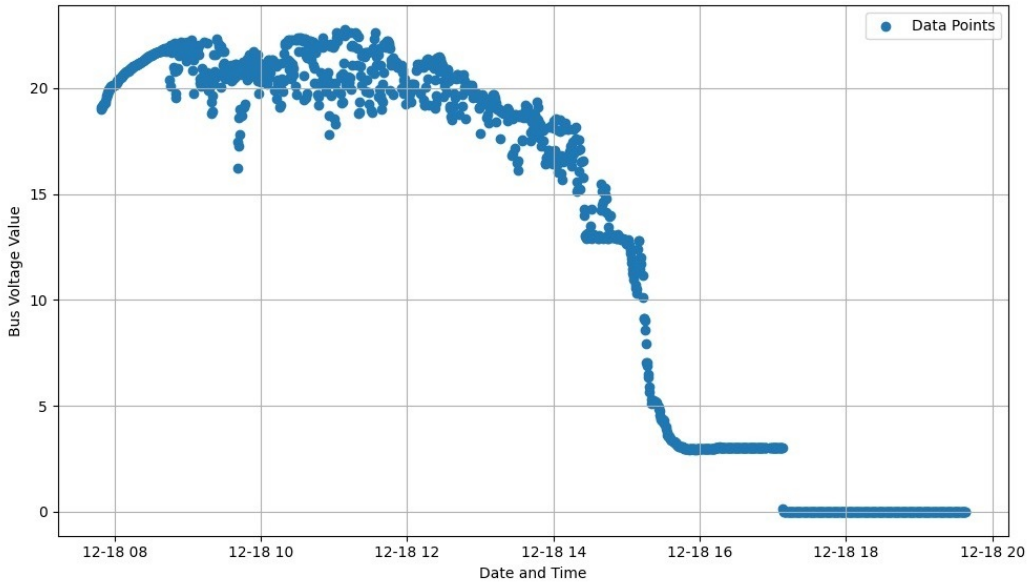

Figure 17. The voltage of the panel on Monday, 18 December 2023 in Lecce influenced by a dynamic environment including sunrise and sunset Figure 14, cloud cover Figure 15, and temperature Figure 16.

The sunrise, occurring at 7:04 (Figure 14), leads to an initial surge in voltage as the test begins, eventually stabilizing at 22 volts, albeit with noticeable noise. This gradual increase can be attributed to the soft, ambient light during the early stages of sunrise, characterized by the sun on the horizon and the lingering twilight effect resulting from the sun's rays reflecting in the atmosphere. This stable condition persists until noon.

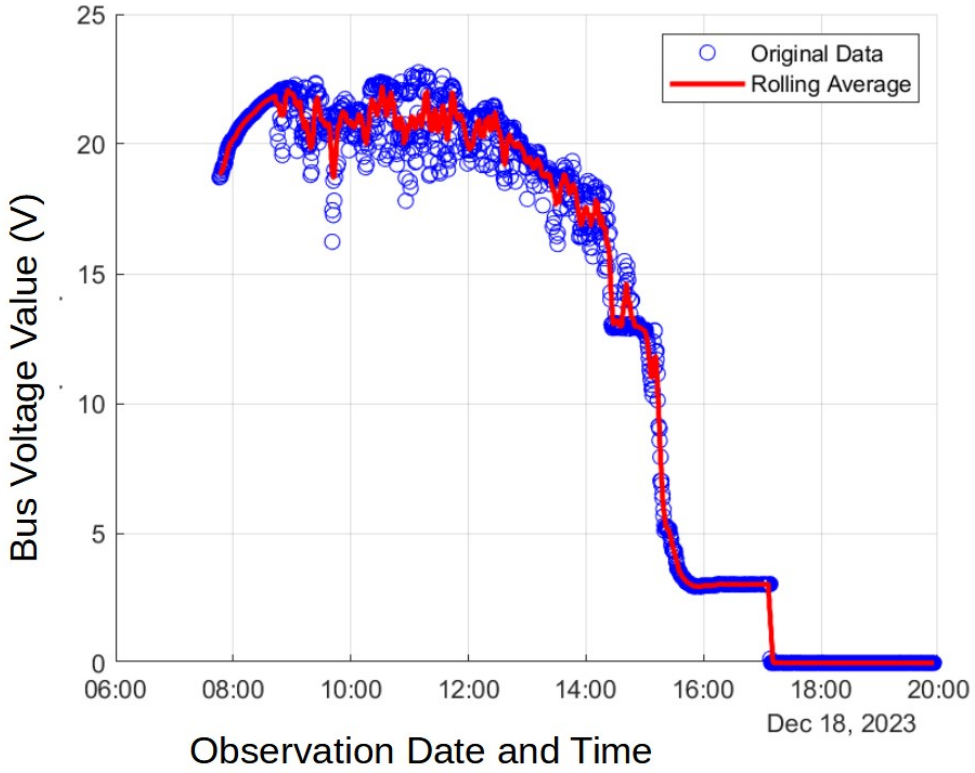

Figure 18. Panel voltage (on Monday, 18 December 2023): comparison between original data and rolling average.

Around 12:00 p.m., cloud cover emerges, introducing a decline in production. By 2:40 p.m., the sky becomes partly cloudy, further impacting the voltage, causing a decrease. As the test progresses towards sunset at 4:22 p.m., and twilight ensues, there is a dramatic effect on production, ultimately stabilizing at 3 volts.

The nocturnal production, observed post-sunset, is attributed to light contamination from the building's surroundings. Yet, such a contamination does not yield any significant contribution to the power output and the system, no longer being able to sustain itself, and keeps operating until the residual battery power is no longer sufficient. At that point, observable at about 17:00, the power suddenly drops as an effect of the lack of power to feed the system. This synthesis affirms the system's functionality under real-world dynamic environmental conditions.

In a nutshell, the comprehensive analysis of the smart PV panel's functionality under real-world dynamic environmental conditions provides a robust understanding of its behavior throughout the day. The system's ability to adapt to varying light intensities, to respond to cloud cover, and to exhibit stability in the presence of noise and light contamination poses it as a reliable and resilient solution for solar energy production in diverse settings. The findings also pave the way for future studies, such as building data-driven or physical models, in order to further enhance our understanding and optimize the system's performance.

In next section, we will identify the disturbance scenario and quantify the resilience of the system using the method detailed in Section 3.1. The Resilience KPIs are scenario-based

indices. For each risk, the R-KPI must be calculated separately. This is essential because the behavior of complex systems following disturbances of varying natures will differ across different scenarios. In this section, the R-KPIs of the system are calculated in the presence of the scenario that is detailed in Section 6.3.

The disturbance was applied at 9:00 a.m. on 18 December 2023. The environmental conditions of the test day are described in Section 6.1. Subsequent subsections provide an explanation of the disturbance scenario and the calculation of R-KPIs for resilience quantification.

6.3. Disturbance Scenario

For the testing phase, we have chosen the False Data Injection risk [92], a scenario characterized by its cybersecurity nature. This selection is motivated by the pervasive adoption of distributed computing in decentralized energy systems, where IoT device networks and smart grids play a crucial role in automating industrial control, modern power systems, and other CIs. This risk is pivotal, as attacks on power systems operating within smart grids lead to the loss of control over management devices, causing operational issues, power outage, and significant power disruptions [93]. These systems heavily rely on sensors and actuators to generate and transmit sensory data through various nodes. While providing substantial benefits for different industries, these systems are vulnerable to cyber-attacks.

False Data Injection Attacks (FDIA) represent a specific category of malicious data attacks targeting CIs managed by Cyber-Physical Information Systems [94], including Digital Twins. FDIA strategies involve attackers compromising sensor readings, introducing undetected corrupt data into calculations of values and variables crucial for defining the system's state. In this particular scenario, the focus is on injecting false angle data into the system.

To simulate the attack, we manually alter the angle of the panel (the direction in which the panel rotates around the horizontal axis) and force the panel to return to its rest angle—the position it assumes when the system is turned off. Following this command, the panel undergoes a change in orientation that deviates from the optimal angle. Consequently, the ideal state service of the Digital Twin, as elucidated in Section 6, should recognize this erroneous position and issue a command to the system to optimize its orientation.

In the subsequent section, we will present and discuss the test results, accompanied by the calculation of R-KPIs.

6.4. Testbed Functionality Validation

The system has been validated in various scenarios, reflecting the impact of variable real-world conditions on the performance of power generation along with validation of mDTs integration with each other and with sensor readings and action commands along with the Communication and Persistence Layer. In the validation scenario discussed in this work, the DT has been set up to update the panel orientation in near real-time to make it face the sun directly (rotating with two DoF in Figure 8). Command messages travel from the Digital Twin to its physical counterpart every minute, and the MPPT is tuned to keep the battery LoC between 10.25 and 10.5 volts. The observations were gathered at a frequency of one batch of sensor data every 30 s over a time span of 30 min. These collections occurred at various times of different days, encompassing an external perimeter, and were conducted under sunny weather conditions, sunny weather conditions with occasional periods of partial cloudiness, and cloudy conditions. As a result, the panel orientation was updated to match the (solar azimuth, solar elevation) couples of angles. For instance, in the sunny sky scenario, the panel spans from (175°, 27°), respectively, to (183°,

27°). The plot illustrated in Figure 19 is a sample of the evolution of PV output voltage and battery level of charge (LoC). The irregular pattern of the PV curve reflects the disturbance introduced by obstacles that cause shading phenomena on the PV panel's surface, which are mainly characterized by the passage of clouds and some external obstacles (a tree). As a result, the curve features a series of steep descents and ascents, but the range of the PV output voltage is still kept relatively small (less than 1 volt) by the MPPT. On the other hand, the curve representing the battery LoC exhibits a saw-tooth profile. In particular, slow descents caused by the execution of edge tasks are interleaved by steep ascents, which will represent the intervention of the MPPT in feeding the battery enough to keep its LoC between the above-mentioned thresholds. A second scenario was simulated to observe the evolution of PV voltage output when the panel's pose is fixed. This test is conducted to have a focused evaluation of the functionality of integrated mDTs with DBMS and IoT elements and to validate the efficacy of the proposed architecture. Figure 20 plots this curve during sunset. The temperature curve is arguably related to the solar exposition intensity, as it smoothly goes down as the position of the sun concerning the solar panel changes. On the other hand, the PV voltage output curve resembles a discrete descending staircase function. This profile is given by the action of the MPPT component, whose function is to regularize the output voltage by tracking the maximum power intensity provided by the PV panel. The results demonstrate that the system of systems yields the anticipated outcomes, and the overall complex system functions efficiently. However, the system is subject to certain limitations, which will be elaborated upon in the next section along with the proposed future steps.

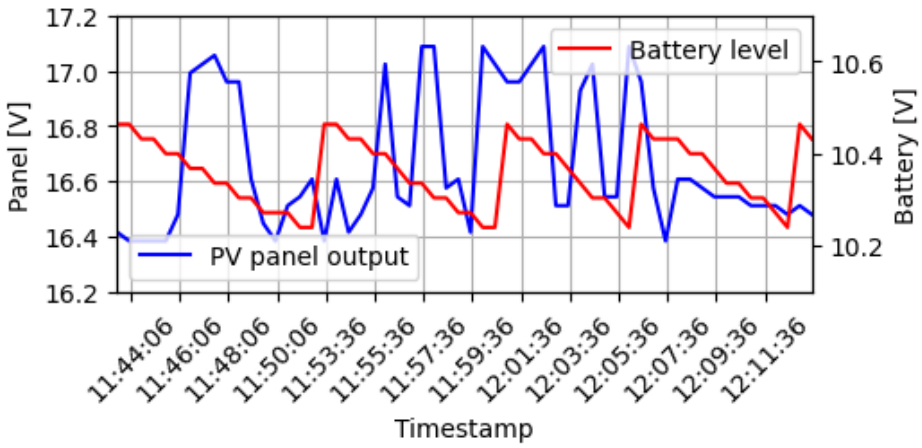

Figure 19. PV panel output and battery level.

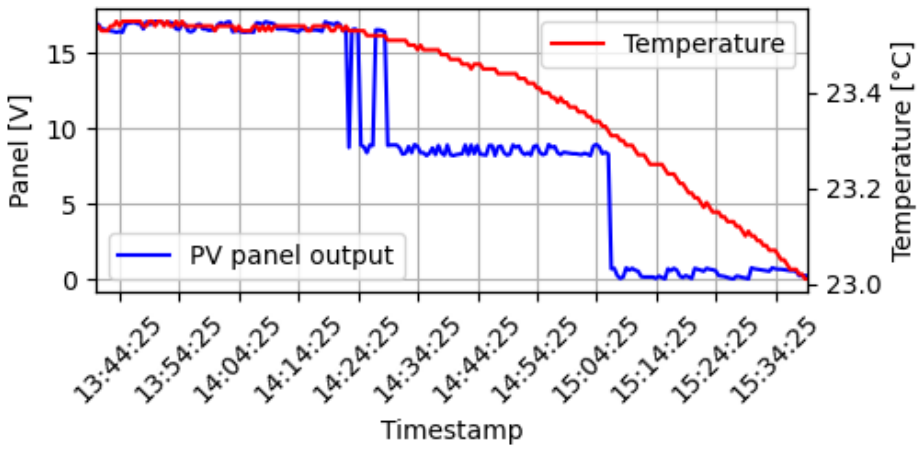

Figure 20. Sunset: PV output and air temperature.

6.5. Resilience Quantification and Synthesis Results

The false position was applied at 9:00 a.m., and as shown in Figure 21, the collected data after the disturbance reveals a decline in voltage starting from 9:00 p.m. Figure 21 provides a clearer depiction of the system's behavior post-disturbance, unveiling its irregular response (Figure 3).

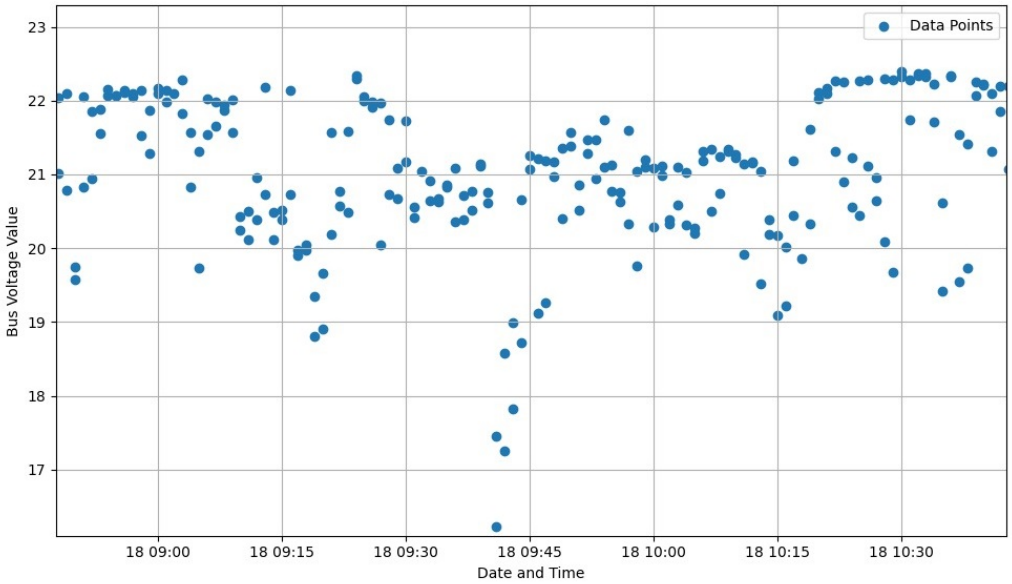

Figure 21. Bus voltage measurement during the disturbance (voltate in volts).

In the initial phase, we can determine the recovery time using Figure 22 as around 10:20 p.m.; the system's behavior stabilizes again, hovering around a panel voltage value of 22 volts. The observed recovery time of 80 min appears to be lengthy. However, it is essential to note that the test was conducted on a testbed constructed with basic elements, with the primary goal being to assess the functionality of the Digital Twin (DT) and establish a sample process for quantifying resilience. Conducting the test in a facility equipped with industrial hardware would likely result in a shorter recovery time.

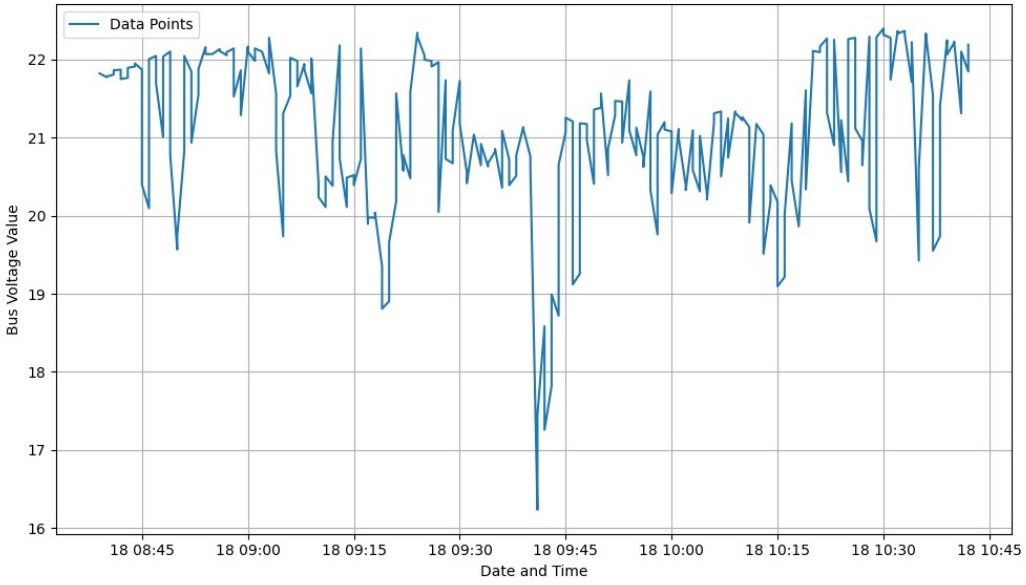

Figure 22. The irregular behaviour of the system after disturbance.

The minimum production level the system reached after the disturbance was 16.1 volts. Although the decrease was dramatic, the system quickly initiated the recovery period and did not linger at the minimum level, showcasing a positive characteristic for a critical infrastructure system.

In this stage, two types of polynomial fitting to the dataset are employed: Support Vector Regression (SVR) and Least Squares. The utilization of these two methods aims to highlight the difference between the straightforward second-degree polynomial least squares calculation and the more intricate SVR, with the objective of overfitting the resilience curve to demonstrate its behavior and calculate the Functionality Loss (Figure 23).

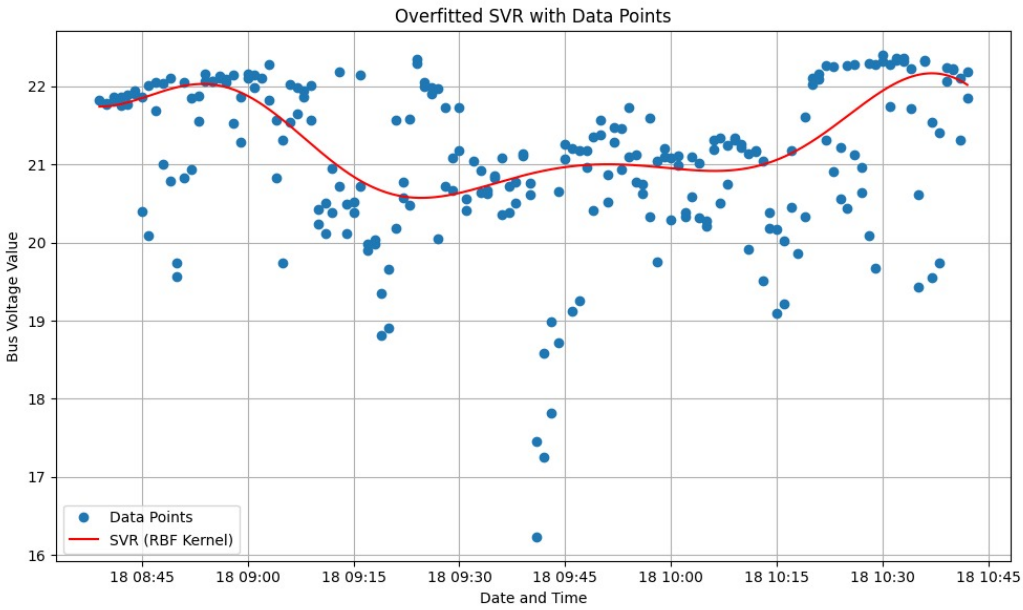

Figure 23. The resilience curve (fitted by SVR).

Even though SVR attempts to fit the curve to the dataset more precisely than least squares, measurements lower than 20.5 volts still do not have an impact on the fitted curve (Figure 23). This is attributed to the closeness of the points and congestion of the measurements above 20.5 volts. However, a more complex solution could involve using the moving average to decrease the density and incorporate the effects of global and local minimums into the fitted curve. Nevertheless, since the system starts to recover very quickly—the global minimum occurs in less than 10 min with values under 19 volts—this additional modification is deemed unnecessary.

Considering that the stable value before the disturbance was 22 volts and the system stabilized again at 22 volts after 10:30 a.m., a horizontal line is considered on the Bus Voltage Value axis (shown in green), and the area between the fitted curve and the horizontal area is calculated (in the figures the area that shows the Functionality Loss is highlighted in yellow). Figures 24 and 25 depict the results.

The results of calculating the Functionality Loss for the Least Squares-fitted resilience curve is 6957.07, and for SVR is 5385.83. The Least Squares-fitted resilience curve shows higher Functionality Loss; however, it does not represent the behavior of system. On the other hand, the SVR curve shows less Functionality Loss. Considering the absence of the global minimum voltage in the SVR curve, the the Least Squares-fitted resilience curve sounds closer to reality. However the graphical representation of the behavior is crucial, and in this case, we select the SVR-fitted resilience curve.

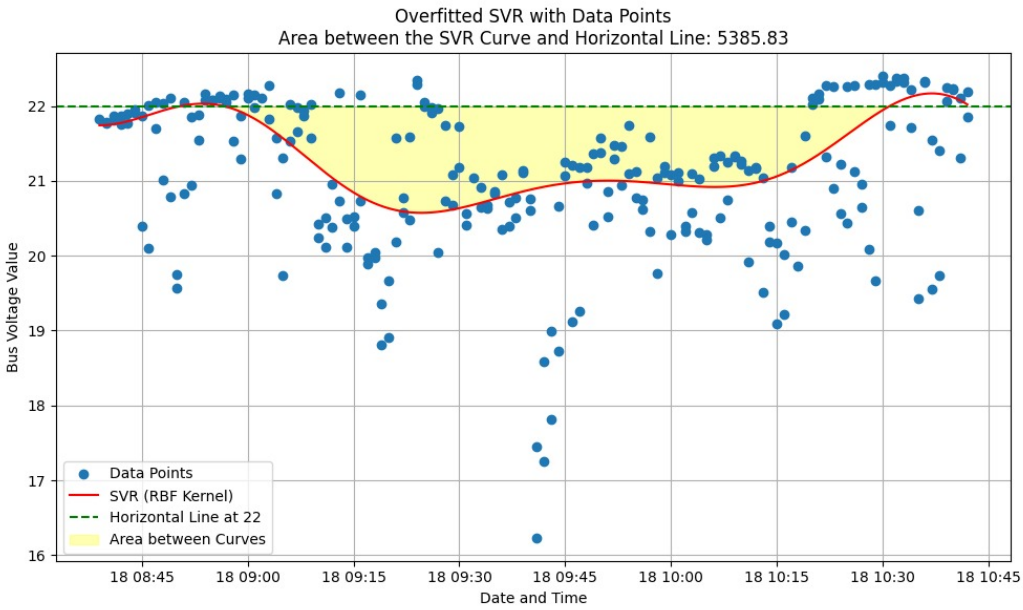

Figure 24. Functionality Loss calculation using the resilience curve fitted by SVR.

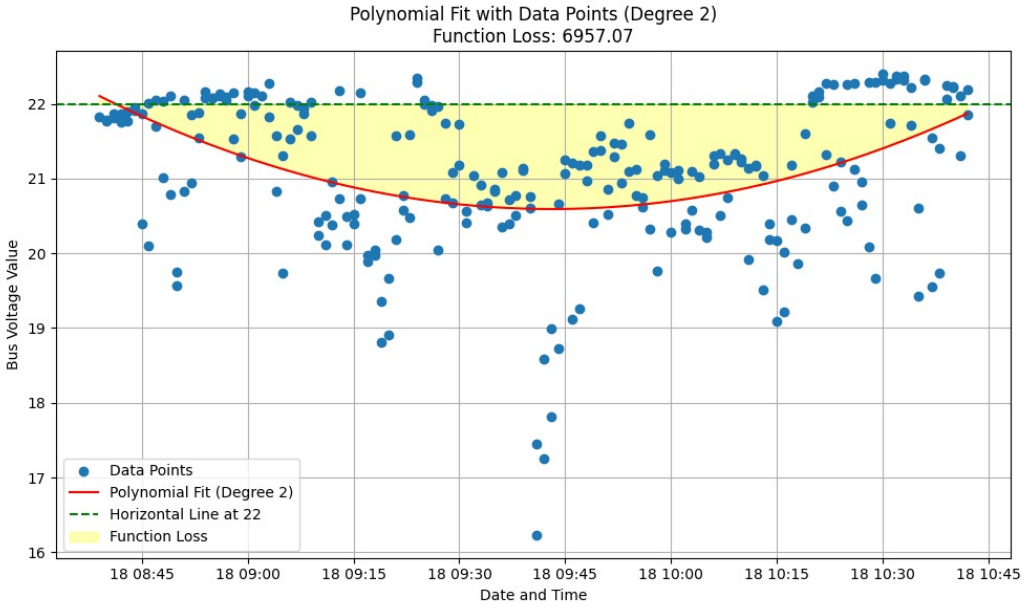

Figure 25. Functionality Loss calculation using the resilience curve fitted by Least Squares.

7. Limitations, Challenges, and Future Study

The current article represents a scoping review of knowledge synthesis. It employs a systematic and iterative approach to identify and report on the existing or emerging body of literature related to the quantification of R-KPIs for modeling critical infrastructure resilience. However, for a more comprehensive analysis, a deeper exploration of real-life cases, extensive discussion, and validation of the reported R-KPIs in the literature require scenario-based validations. This, therefore, stands as a potential avenue for future research.

Similarly, the prioritization of R-KPIs also necessitates a scenario-based approach and an in-depth examination through real-life case studies, criteria extraction, and R-KPI prioritization. Unfortunately, there is currently no literature available that identifies the criteria for critical infrastructure resilience in a general context. This study has the potential to pave the way for future research to fill this gap and further enrich the knowledge base for the quantitative modeling of critical infrastructure resilience.

Finally, future studies should investigate the challenges associated with highly noisy real-time data from embedded sensors, as this is a common occurrence in real-world scenarios involving diverse machine types. In the current study, the sensors provide data with relatively low natural noise. However, the issue of highly noisy data is a potential topic for future research.

8. Conclusions

In conclusion, this study has successfully addressed the critical question of real-time resilience monitoring for IoT-integrated CIs. By developing and validating a robust framework, this research contributes significantly to the resilience engineering domain. The integration of R-KPIs, including Functionality Loss, Minimum Performance, and Recovery Time, has enabled a targeted approach to resilience quantification. Using a Digital Twin-integrated smart PV panel, we demonstrated the effectiveness of IoT-based, real-time monitoring for assessing the resilience of cyber-physical systems under simulated disturbances.

The findings underscore the importance of continuous, real-time data acquisition in supporting actionable insights for resilience enhancement, providing a systematic approach to resilience quantification for CIs. This framework and testbed model are not only practical but also reusable, offering researchers and industry professionals a solid foundation for further resilience studies in IoT-integrated infrastructures. These contributions advance resilience monitoring, support secure service continuity, and address the growing need for robust resilience in essential services, paving the way for more resilient, IoT-enabled infrastructures that can better withstand and recover from future disturbances.

Author Contributions: A.A.A. contributed in the research project from inception to final manuscript preparation, including conceptualization, experimental design, data analysis, and drafting along with coordination of the team. A.L. provided essential supervision and guidance throughout the study, shaping its direction. C.M. constructed and managed the experimental testbed, ensuring functionality, reliability, and overseeing data collection. C.R. conducted the state-of-the-art review and contributed to manuscript drafting. A.F. supported the project through supervision and administrative oversight. F.I. contributed to the development of immersive environments and user interfaces in Unreal Engine. All authors have read and agreed to the published version of the manuscript.

Funding: This research received no external funding.

Institutional Review Board Statement: Not applicable.

Informed Consent Statement: Not applicable.

Data Availability Statement: The data presented in this study are available on request from the corresponding author. The raw data supporting the conclusions of this article will be made available on request.

Conflicts of Interest: Author Ali Aghazadeh Ardebili was employed by the company HSPI SpA. The remaining authors declare that the research was conducted in the absence of any commercial or financial relationships that could be construed as a potential conflict of interest.

References

1. Radanliev, P.; De Roure, D.; Van Kleek, M.; Santos, O.; Ani, U. Artificial intelligence in cyber physical systems. *AI Soc.* **2020**, *36*, 783–796. [CrossRef] [PubMed]
2. Batista e Silva, F.; Forzieri, G.; Marin Herrera, M.A.; Bianchi, A.; Lavalle, C.; Feyen, L. HARCI-EU, a harmonized gridded dataset of critical infrastructures in Europe for large-scale risk assessments. *Sci. Data* **2019**, *6*, 126. [CrossRef] [PubMed]
3. Cantelmi, R.; Di Gravio, G.; Patriarca, R. Reviewing qualitative research approaches in the context of critical infrastructure resilience. *Environ. Syst. Decis.* **2021**, *41*, 341–376. [CrossRef] [PubMed]

4. Akakura, Y.; Sasaki, T.; Ono, K.; Watanabe, T. An Assessment of the Impacts on the International Container Transport and the World Economy Resulting from the 2014/15 U.S. West Coast Port Disruption. *J. Integr. Disaster Risk Manag.* **2018**, *8*, 1–21. [CrossRef]
5. Gallarno, G.; Muniz, J.; Parnell, G.S.; Pohl, E.A.; Wu, J. Development and assessment of a resilient telecoms system. *J. Def. Model. Simul. Appl. Methodol. Technol.* **2023**, *21*, 405–420. [CrossRef]
6. Koks, E.; Pant, R.; Thacker, S.; Hall, J.W. Understanding Business Disruption and Economic Losses Due to Electricity Failures and Flooding. *Int. J. Disaster Risk Sci.* **2019**, *10*, 421–438. [CrossRef]
7. Avordeh, T.K.; Salifu, A.; Quaidoo, C.; Opare-Boateng, R. Impact of power outages: Unveiling their influence on micro, small, and medium-sized enterprises and poverty in Sub-Saharan Africa - An in-depth literature review. *Heliyon* **2024**, *10*, e33782. [CrossRef]
8. Zhu, Q.; Başar, T. Disentangling Resilience From Robustness: Contextual Dualism, Interactionism, and Game-Theoretic Paradigms. *IEEE Control. Syst. Mag.* **2024**, *44*, 95–103. [CrossRef]
9. Xu, L.; Guo, Q.; Sheng, Y.; Muyeen, S.; Sun, H. On the resilience of modern power systems: A comprehensive review from the cyber-physical perspective. *Renew. Sustain. Energy Rev.* **2021**, *152*, 111642. [CrossRef]
10. Kwasinski, A. Modeling of Cyber-Physical Intra-Dependencies in Electric Power Grids and Their Effect on Resilience. In Proceedings of the 2020 8th Workshop on Modeling and Simulation of Cyber-Physical Energy Systems, Sydney, Australia, 21 April 2020; pp. 1–6. [CrossRef]
11. Urlainis, A.; Ornai, D.; Levy, R.; Vilnay, O.; Shohet, I.M. Loss and damage assessment in critical infrastructures due to extreme events. *Saf. Sci.* **2022**, *147*, 105587. [CrossRef]
12. Loveček, T.; Straková, L.; Kampová, K. Modeling and Simulation as Tools to Increase the Protection of Critical Infrastructure and the Sustainability of the Provision of Essential Needs of Citizens. *Sustainability* **2021**, *13*, 5898. [CrossRef]
13. Carrington, N.K.; Ma, S.; Dobson, I.; Wang, Z. Extracting Resilience Statistics from Utility Data in Distribution Grids. In Proceedings of the 2020 IEEE Power & Energy Society General Meeting (PESGM), Montreal, QC, Canada, 2–6 August 2020; pp. 1–5. [CrossRef]
14. Fuggini, C.; Bolletta, F. Identification of indicators, metrics and level of service for the resilience of transport critical infrastructure. *Int. J. Sustain. Mater. Struct. Syst.* **2020**, *4*, 330. [CrossRef]
15. Achillopoulou, D.V.; Mitoulis, S.A.; Argyroudis, S.A.; Wang, Y. Monitoring of transport infrastructure exposed to multiple hazards: A roadmap for building resilience. *Sci. Total Environ.* **2020**, *746*, 141001. [CrossRef] [PubMed]
16. Aghazadeh Ardebili, A.; Ficarella, A.; Longo, A.; Mazzeo, O. Critical Infrastructure Resilience. 2023. Available online: https://iris.unisalento.it/handle/11587/503626 (accessed on 3 December 2024).
17. Aghazadeh Ardebili, A.; Padoano, E. A literature review of the concepts of resilience and sustainability in group decision-making. *Sustainability* **2020**, *12*, 2602. [CrossRef]
18. Chaterji, S.; Naghizadeh, P.; Alam, M.A.; Bagchi, S.; Chiang, M.; Corman, D.; Henz, B.; Jana, S.; Li, N.; Mou, S.; et al. Resilient cyberphysical systems and their application drivers: A technology roadmap. *arXiv* **2019**, arXiv:2001.00090.
19. Ardebili, A.A.; Longo, A.; Ficarella, A. Implementing Digital Twins in Energy Systems: Meta Analysis of the State of Art and Evolution. 2021. Available online: https://www.semanticscholar.org/paper/Implementing-Digital-Twins-in-Energy-Systems%3A-Meta-Ardebili-Longo/16e088485affb69bd5c5b4f88bb7b68c08bd8a4a (accessed on 3 December 2024).
20. Ardebili, A.A.; Longo, A.; Ficarella, A. Digital Twins bonds society with cyber-physical Energy Systems: A literature review. In Proceedings of the 2021 IEEE International Conferences on Internet of Things (iThings) and IEEE Green Computing & Communications (GreenCom) and IEEE Cyber, Physical & Social Computing (CPSCom) and IEEE Smart Data (SmartData) and IEEE Congress on Cybermatics (Cybermatics), Melbourne, Australia, 6–8 December 2021; pp. 284–289.
21. Habibi Rad, M.; Mojtahedi, M.; Ostwald, M.J. Industry 4.0, disaster risk management and infrastructure resilience: A systematic review and bibliometric analysis. *Buildings* **2021**, *11*, 411. [CrossRef]
22. Ye, X.; Du, J.; Han, Y.; Newman, G.; Retchless, D.; Zou, L.; Ham, Y.; Cai, Z. Developing human-centered urban digital twins for community infrastructure resilience: A research agenda. *J. Plan. Lit.* **2023**, *38*, 187–199. [CrossRef]
23. Argyroudis, S.A.; Mitoulis, S.A.; Chatzi, E.; Baker, J.W.; Brilakis, I.; Gkoumas, K.; Vousdoukas, M.; Hynes, W.; Carluccio, S.; Keou, O.; et al. Digital technologies can enhance climate resilience of critical infrastructure. *Clim. Risk Manag.* **2022**, *35*, 100387. [CrossRef]
24. Geels, F.W. Transformative innovation and socio-technical transitions to address grand challenges. *Eur. Comm. R&I Pap. Ser. Work. Pap.* **2020**, *2*, 1–39.
25. Rohracher, H. 45Analyzing the Socio-Technical Transformation of Energy Systems: The Concept of Sustainability Transitions. In *Oxford Handbook of Energy and Society*; Oxford University Press: Oxford, UK, 2018.
26. Guelpa, E.; Bischi, A.; Verda, V.; Chertkov, M.; Lund, H. Towards future infrastructures for sustainable multi-energy systems: A review. *Energy* **2019**, *184*, 2–21. [CrossRef]

27. Aghazadeh Ardebili, A.; Zappatore, M.; Ramadan, A.I.H.A.; Longo, A.; Ficarella, A. Digital Twins of smart energy systems: A systematic literature review on enablers, design, management and computational challenges. *Energy Inform.* **2024**, *7*, 94. [CrossRef]
28. Ardebili, A.A.; Longo, A.; Ficarella, A. Navigating the Future Data-Driven Automation Tools: State-of-the-Art and Research Roadmap for Digital Twins of Energy Systems. In Proceedings of the 2023 IEEE International Conference on Big Data (BigData), Sorrento, Italy, 15–18 December 2023; pp. 3888–3897.
29. Aghazadeh Ardebili, A.; Hasidi, O.; Bendaouia, A.; Khalil, A.; Khalil, S.; Luceri, D.; Longo, A.; Abdelwahed, E.H.; Qassimi, S.; Ficarella, A. Enhancing resilience in complex energy systems through real-time anomaly detection: A systematic literature review. *Energy Inform.* **2024**, *7*, 96. [CrossRef]
30. Zhou, K.; Yang, S. Understanding household energy consumption behavior: The contribution of energy big data analytics. *Renew. Sustain. Energy Rev.* **2016**, *56*, 810–819. [CrossRef]
31. Zhou, K.; Fu, C.; Yang, S. Big data driven smart energy management: From big data to big insights. *Renew. Sustain. Energy Rev.* **2016**, *56*, 215–225. [CrossRef]
32. Ma, Z.; Xie, J.; Li, H.; Sun, Q.; Si, Z.; Zhang, J.; Guo, J. The role of data analysis in the development of intelligent energy networks. *IEEE Netw.* **2017**, *31*, 88–95. [CrossRef]
33. Johansson, B. Security aspects of future renewable energy systems–A short overview. *Energy* **2013**, *61*, 598–605. [CrossRef]
34. Sadorsky, P. Some future scenarios for renewable energy. *Futures* **2011**, *43*, 1091–1104. [CrossRef]
35. Bessa, R.; Moreira, C.; Silva, B.; Matos, M. Handling renewable energy variability and uncertainty in power system operation. In *Advances in Energy Systems: The Large-Scale Renewable Energy Integration Challenge*; John Wiley & Sons: Hoboken, NJ, USA, 2019; pp. 1–26.
36. Jafarizadeh, H.; Yamini, E.; Zolfaghari, S.M.; Esmaeilion, F.; Assad, M.E.H.; Soltani, M. Navigating challenges in large-scale renewable energy storage: Barriers, solutions, and innovations. *Energy Rep.* **2024**, *12*, 2179–2192. [CrossRef]
37. Bremen, L.V. Large-scale variability of weather dependent renewable energy sources. In *Management of Weather and Climate Risk in the Energy Industry*; Springer: Berlin/Heidelberg, Germany, 2010; pp. 189–206.
38. Zhao, A.P.; Li, S.; Gu, C.; Yan, X.; Hu, P.J.H.; Wang, Z.; Xie, D.; Cao, Z.; Chen, X.; Wu, C.; et al. Cyber vulnerabilities of energy systems. *IEEE J. Emerg. Sel. Top. Ind. Electron.* **2024**, *5*, 1455–1469. [CrossRef]
39. Demertzis, K.; Iliadis, L. A computational intelligence system identifying cyber-attacks on smart energy grids. In *Modern Discrete Mathematics and Analysis: With Applications in Cryptography, Information Systems and Modeling*; Springer: Berlin/Heidelberg, Germany, 2018; pp. 97–116.
40. Sridhar, S.; Hahn, A.; Govindarasu, M. Cyber-Physical Systems Security for the Electric Power Grid. *Proc. IEEE* **2012**, *100*, 250–266. [CrossRef]
41. Yang, Y.; Du, H.; Xiong, Z.; Xu, R.; Niyato, D.; Han, Z. Exploring Impacts of Age of Information on Data Accuracy for Wireless Sensing Systems: An Information Entropy Perspective. *IEEE Trans. Mob. Comput.* **2025**, 1–18. [CrossRef]
42. Kahraman, I.; Köse, A.; Koca, M.; Anarim, E. Age of information in internet of things: A survey. *IEEE Internet Things J.* **2023**, *11*, 9896–9914. [CrossRef]
43. Zhang, T.; Zhou, J.; Chen, Z.; Tian, Z.; Wen, W.; Jia, Y. Information freshness optimization of multiple status update streams in Internet of things: Generation rate control and service rate reservation. *Digit. Commun. Netw.* **2023**, *9*, 971–980. [CrossRef]
44. Liu, X.; Liu, H.; Zheng, K.; Liu, J.; Taleb, T.; Shiratori, N. AoI-Minimal Clustering, Transmission and Trajectory Co-Design for UAV-Assisted WPCNs. *IEEE Trans. Veh. Technol.* **2025**, *74*, 1035–1051. [CrossRef]
45. Aghazadeh Ardebili, A.; Martella, C.; Martella, A.; Lazari, A.; Longo, A.; Ficarella, A. Smart critical infrastructures security management and governance: Implementation of cyber resilience kpis for decentralized energy asset. In Proceedings of the CEUR Workshop Proceedings-Italian Conference on Cyber Security 2024: Proceedings of the 8th Italian Conference on Cyber Security (ITASEC 2024), Salerno, Italy, 8–12 April 2024; Volume 3731.
46. Poulin, C.; Kane, M.B. Infrastructure resilience curves: Performance measures and summary metrics. *Reliab. Eng. Syst. Saf.* **2021**, *216*, 107926. [CrossRef]
47. Aghazadeh Ardebili, A.; Boscolo, M.; Ficarella, A.; Longo, A.; Padoano, E. Resilience Modeling of Cyber-Physical Systems: A Comparative Study of Statistical vs. AI Methods. In Proceedings of the XXIX AIDI Summer School "Francesco Turco" Industrial Systems Engineering, Lecce, Italy, 11–13 September 2024.
48. Fanucchi, R.; Bessani, M.; Camillo, M.H.; Soares, A.D.S.; London, J.B., Jr.; Desuó, L.; Maciel, C.D. Stochastic indexes for power distribution systems resilience analyzes. *IET Gener. Transmn. Distrib.* **2019**, *13*, 2507–2516. [CrossRef]
49. Ji, A.; He, R.; Chen, W.; Zhang, L. Computational methodologies for critical infrastructure resilience modeling: A review. *Adv. Eng. Inform.* **2024**, *62*, 102663. [CrossRef]
50. Ioannidis, C.; Pym, D.; Williams, J.; Gheyas, I. Resilience in information stewardship. *Eur. J. Oper. Res.* **2019**, *274*, 638–653. [CrossRef]

51. Rezvani, S.M.; Silva, M.J.F.; de Almeida, N.M. Urban Resilience Index for Critical Infrastructure: A Scenario-Based Approach to Disaster Risk Reduction in Road Networks. *Sustainability* **2024**, *16*, 4143. [CrossRef]
52. Kavousi-Fard, A.; Wang, M.; Su, W. Stochastic resilient post-hurricane power system recovery based on mobile emergency resources and reconfigurable networked microgrids. *IEEE Access* **2018**, *6*, 72311–72326. [CrossRef]
53. Bao, S.; Zhang, C.; Ouyang, M.; Miao, L. An integrated tri-level model for enhancing the resilience of facilities against intentional attacks. *Ann. Oper. Res.* **2019**, *283*, 87–117. [CrossRef]
54. Wang, C. Role of recovery profile dependency in time-dependent resilience. *Eng. Rep.* **2024**, *6*, e12716. [CrossRef]
55. Miles, S.; Ly, M.; Terry, N.; Choe, Y. Restimate: Recovery Estimation Tool for Resilience Planning. *J. Saf. Sci. Resil.* **2024**, *5*, 47–63. [CrossRef]
56. Zhang, J.; Li, G.; Zhang, M. Multi-objective optimization for community building group recovery scheduling and resilience evaluation under earthquake. *Comput.-Aided Civ. Infrastruct. Eng.* **2023**, *38*, 1657–1676. [CrossRef]
57. Liang, H.; Xie, Q. Resilience-based sequential recovery planning for substations subjected to earthquakes. *IEEE Trans. Power Deliv.* **2022**, *38*, 353–362. [CrossRef]
58. Lee, S.; Shin, S.; Judi, D.; McPherson, T.; Burian, S. Criticality analyzes of a water distribution system considering both economic consequences and hydraulic loss using modern portfolio theory. *Water* **2019**, *11*, 1222. [CrossRef]
59. Liu, X.; Ferrario, E.; Zio, E. Identifying resilient-important elements in interdependent critical infrastructures by sensitivity analyzes. *Reliab. Eng. Syst. Saf.* **2019**, *189*, 423–434. [CrossRef]
60. Li, R.; Gao, Y. On the component resilience importance measures for infrastructure systems. *Int. J. Crit. Infrastruct. Prot.* **2022**, *36*, 100481. [CrossRef]
61. Lin, S.; El-Tawil, S. Time-dependent resilience assessment of seismic damage and restoration of interdependent lifeline systems. *J. Infrastruct. Syst.* **2020**, *26*, 04019040. [CrossRef]
62. Nozhati, S.; Ellingwood, B.; Chong, E. Stochastic optimal control methodologies in risk-informed community resilience planning. *Struct. Saf.* **2020**, *84*, 101920. [CrossRef]
63. Trucco, P.; Petrenj, B. Characterisation of resilience metrics in full-scale applications to interdependent infrastructure systems. *Reliab. Eng. Syst. Saf.* **2023**, *235*, 109200. [CrossRef]
64. Ouyang, M.; Liu, C.; Xu, M. Value of resilience-based solutions on critical infrastructure protection: Comparing with robustness-based solutions. *Reliab. Eng. Syst. Saf.* **2019**, *190*, 106506. [CrossRef]
65. Panteli, M.; Trakas, D.; Mancarella, P.; Hatziargyriou, N. Power systems resilience assessment: Hardening and smart operational enhancement strategies. *Proc IEEE* **2017**, *105*, 1202–1213. [CrossRef]
66. Pagano, A.; Pluchinotta, I.; Giordano, R.; Vurro, M. Drinking water supply in resilient cities: Notes from L'Aquila earthquake case study. *Sustain. Cities Soc.* **2017**, *28*, 435–449. [CrossRef]
67. Jovanović, A.; Klimek, P.; Renn, O.; Schneider, R.; Øien, K.; Brown, J.; DiGennaro, M.; Liu, Y.; Pfau, V.; Jelić, M.; et al. Assessing resilience of healthcare infrastructure exposed to COVID-19: Emerging risks, resilience indicators, interdependencies and international standards. *Environ. Syst. Decis.* **2020**, *40*, 252–286. [CrossRef]
68. Rosales-Asensio, E.; Elejalde, J.L.; Pulido-Alonso, A.; Colmenar-Santos, A. Resilience framework, methods, and metrics for the prioritization of critical electrical grid customers. *Electronics* **2022**, *11*, 2246. [CrossRef]
69. González, C.; Niño, M.; Ayala, G. Functionality Loss and Recovery Time Models for Structural Elements, Non-Structural Components, and Delay Times to Estimate the Seismic Resilience of Mexican School Buildings. *Buildings* **2023**, *13*, 1498. [CrossRef]
70. Brown, R.G. *Smoothing, Forecasting and Prediction of Discrete Time Series*; Prentice-Hall: Hoboken, NJ, USA, 1963.
71. Chatfield, C. *Time-Series Forecasting*; CRC Press: Boca Raton, FL, USA, 2000.
72. Murphy, J.J. *Technical Analysis of the Financial Markets: A Comprehensive Guide to Trading Methods and Applications*; Penguin: London, UK, 1999.
73. Maddala, G.S. *Introduction to Econometrics*; Wiley: Hoboken, NJ, USA, 2001.
74. Shaker, H.; Alba, E. Noise modeling for photovoltaic systems using real-world data. *IEEE Trans. Sustain. Energy* **2017**, *8*, 1–10.
75. Korpela, T.; Rossi, M.; Lehtonen, M. Noise and signal interference in photovoltaic power data. *Renew. Energy* **2016**, *92*, 139–150.
76. Pratama, I.; Prasetyaningrum, P.T.; Setyaningsih, P.W. Time-Series Data Forecasting and Approximation with Smoothing Technique. In Proceedings of the 2019 International Conference on Information and Communications Technology (ICOIACT), Yogyakarta, Indonesia, 24–25 July 2019; pp. 439–444.
77. Li, D.; Yu, X.; Chen, J.; Lin, Z.; He, S.; Liu, J.; Yao, Y.; Wu, Y. Typical Load Analysis and Forecast of a Provincial Power Grid in Mid-Southern China. In Proceedings of the 2021 IEEE 5th Conference on Energy Internet and Energy System Integration (EI2), Taiyuan, China, 22–24 October 2021; pp. 3352–3357.
78. Raj, R.P.; Kowli, A. Characterizing the ramps and noise in solar power imbalances. *Sol. Energy* **2022**, *247*, 531–542. [CrossRef]
79. Ernst, B.; Wan, Y.H.; Kirby, B. *Short-Term Power Fluctuation of Wind Turbines: Analyzing Data from the German 250-MW Measurement Program from the Ancillary Services Viewpoint*; Technical Report; National Renewable Energy Lab.(NREL): Golden, CO, USA, 1999.

80. Chhabra, M.; Lim, M.; Barnes, F. Frequency stabilization using solar smoothing, leveling and time shifting in a hybrid renewablenetwork. In Proceedings of the ISGT2011-India, Kollam, Kerala, India, 1–3 December 2011; pp. 275–281.
81. Hyndman, R.J.; Athanasopoulos, G. *Forecasting: Principles and Practice*; OTexts: Melbourne, Australia, 2018.
82. Ardebili, A.A.; Martella, A.; Martella, C.; Longo, A.; Ficarella, A. Digital Twins: Case Study of Energy Metaverse and Edge-Cloud Integration. In Proceedings of the 2024 IEEE International Conference on Big Data (BigData), Washington, DC, USA, 15–18 December 2024; pp. 5476–5485. [CrossRef]
83. Chai, B.X.; Gunaratne, M.; Ravandi, M.; Wang, J.; Dharmawickrema, T.; Di Pietro, A.; Jin, J.; Georgakopoulos, D. Smart industrial internet of things framework for composites manufacturing. *Sensors* **2024**, *24*, 4852. [CrossRef] [PubMed]
84. Yılmaz, N.; Alatlı, O.; Çiloğlugil, B.; Erdur, R.C. Evaluation of storage and query performance of sensor based Internet of Things data with MongoDB. In Proceedings of the 2018 International Conference on Artificial Intelligence and Data Processing (IDAP), Malatya, Turkey, 28–30 September 2018; pp. 1–6.
85. Pandey, R. Performance Benchmarking and Comparison of Cloud-Based Databases MongoDB (NoSQL) vs. MySQL (Relational) Using YCSB. *Electron. Resour.* **2020**. Available online: https://www.researchgate.net/publication/344047197_Performance_Benchmarking_and_Comparison_of_Cloud-Based_Databases_MongoDB_NoSQL_Vs_MySQL_Relational_using_YCSB (accessed on 3 December 2024).
86. Eyada, M.M.; Saber, W.; El Genidy, M.M.; Amer, F. Performance evaluation of IoT data management using MongoDB versus MySQL databases in different cloud environments. *IEEE Access* **2020**, *8*, 110656–110668. [CrossRef]
87. Ardebili, A.A.; Longo, A.; Ficarella, A. Digital twinning of PV modules for smart systems-A comparison between commercial and open-source simulation models. In Proceedings of the 2023 IEEE International Conference on Dependable, Autonomic and Secure Computing, International Conference on Pervasive Intelligence and Computing, Intl Conf on Cloud and Big Data Computing, Intl Conf on Cyber Science and Technology Congress (DASC/PiCom/CBDCom/CyberSciTech), Abu Dhabi, United Arab Emirates, 14–17 November 2023; pp. 1045–1050.
88. Aghazadeh Ardebili, A.; Ficarella, A.; Longo, A.; Khalil, A.; Khalil, S. Hybrid Turbo-Shaft Engine Digital Twinning for Autonomous Aircraft via AI and Synthetic Data Generation. *Aerospace* **2023**, *10*, 683. [CrossRef]
89. Aghazadeh Ardebili, A.; Longo, A.; Ficarella, A.; Khalil, A.; Khalil, S. Exploring Synthetic Noise Algorithms for Real-World Similar Data Generation: A Case Study on Digitally Twining Hybrid Turbo-Shaft Engines in UAV/UAS Applications. In *Model and Data Engineering: Proceedings of the 12th International Conference (MEDI 2023), Sousse, Tunisia, 2–4 November 2023*; Springer: Cham, Switzerland, 2023; pp. 87–101.
90. The European Commission. European Industrial Technology Roadmap for the Next Generation Cloud-Edge Offering. Technical Report. 2021. Available online: https://ec.europa.eu/newsroom/repository/document/2021-18/European_CloudEdge_Technology_Investment_Roadmap_for_publication_pMdz85DSw6nqPppq8hE9S9RbB8_76223.pdf (accessed on 3 December 2024).
91. Somma, A.; Benedictis, A.D.; Zappatore, M.; Martella, C.; Martella, A.; Longo, A. Digital Twin Space: The Integration of Digital Twins and Data Spaces. In Proceedings of the 2023 IEEE International Conference on Big Data (BigData), Sorrento, Italy, 15–18 December 2023; pp. 4017–4025. [CrossRef]
92. Yong, S.Z.; Zhu, M.; Frazzoli, E. Switching and data injection attacks on stochastic cyber-physical systems: Modeling, resilient estimation, and attack mitigation. *ACM Trans. Cyber-Phys. Syst.* **2018**, *2*, 1–2. [CrossRef]
93. Tan, R.; Nguyen, H.H.; Yau, D.K. Collaborative load management with safety assurance in smart grids. *ACM Trans. Cyber-Phys. Syst.* **2017**, *1*, 1–27. [CrossRef]
94. Matei, I.; Piotrowski, W.; Perez, A.; de Kleer, J.; Tierno, J.; Mungovan, W.; Turnewitsch, V. System resilience through health monitoring and reconfiguration. *ACM Trans. Cyber-Phys. Syst.* **2024**, *8*, 1–27. [CrossRef]